ELSEVIER

Journal of Structural Geology 27 (2005) 1899–1924

JOURNAL OF STRUCTURAL GEOLOGY

www.elsevier.com/locate/jsg

U–Th–Pb geochronologic constraints on the structural evolution of the Selkirk fan, northern Selkirk Mountains, southern Canadian Cordillera

H. Daniel Gibson*, Richard L. Brown, Sharon D. Carr

Department of Earth Sciences, Carleton University, Ottawa, ON, Canada K1S 5B6

Received 6 November 2003; received in revised form 17 May 2005; accepted 20 May 2005
Available online 8 August 2005

Abstract

In the southern Canadian Cordillera a zone of structural divergence marks the eastward transition from penetrative ductile deformation and metamorphism in the Omineca belt to the more brittle 'thin-skinned' style of deformation typical of the Foreland belt. In the Selkirk Mountains of southern British Columbia, this zone includes a regional-scale structure termed the Selkirk fan. The fan trends northwest, consists primarily of medium- to high-grade metamorphic rocks, and comprises at least three generations of superposed structures. IDTIMS and SHRIMP analyses provide new U–Th–Pb age constraints for the structural evolution of the Selkirk fan. The data demonstrate that the thermo-structural development of the fan's west flank occurred principally in the Middle Jurassic (ca. 172–167 Ma), whereas in the east flank significant Cretaceous (ca. 104–84 Ma) deformation was superimposed on an early transposition fabric. These data require revision of previous models that concluded fan formation occurred primarily during Middle Jurassic time. Rather, the Selkirk fan is a composite structure comprising Middle Jurassic and Cretaceous deformation. Development of the fan during the Early–Middle Jurassic accretion of the Intermontane Superterrane was followed by extensive reworking and tightening of structures in the fan's east flank during the Cretaceous accretion of the Insular Superterrane.

Keywords: Structural fan; Canadian Cordillera; U–Th–Pb geochronology; IDTIMS; SHRIMP; Diachronous deformation

1. Introduction

The Omineca belt of the Canadian Cordillera (Fig. 1a) was the locus of ductile deformation, metamorphism and plutonism during the Mesozoic accretion of the Intermontane and Insular superterranes to the western margin of North America (Monger et al., 1982; Murphy et al., 1995). The eastward transition from rocks affected by deep-seated ductile and metamorphic processes in the southern Omineca belt to the 'thin-skinned' deformation of the Foreland belt is marked by a regional zone of structural divergence (Fig. 1a). From west to east, this represents a reversal from southwest- to northeast-vergent structures; the axis of this zone can be traced northward along the entire length of the Canadian Cordillera, and on into Alaska (Price, 1986, and references therein). Understanding the development of this orogen-scale divergence is fundamental to elucidating the transition from hinterland to foreland tectonics in the Cordillera.

In the Selkirk Mountains of southern British Columbia, within the southern Omineca belt, part of the zone of structural divergence coincides with a regional-scale structure termed the Selkirk fan (Wheeler, 1963, 1965; Price and Mountjoy, 1970; Brown and Tippett, 1978) (Figs. 1b and 2a). The fan trends northwest–southeast for more than 120 km, is composed of low- to high-grade metamorphic rocks, and comprises at least three generations of superposed structures. The kinematic development of the Selkirk fan has been the focus of considerable debate from which two principal tectonic models have emerged. Brown et al. (1993) presented a finite-element model, suggesting that the fan developed above a singularity that marked the eastward subduction of oceanic or marginal basin lithosphere beneath continental lithosphere (Fig. 2b). This is analogous to the mechanical models of Malavieille (1984) and Willett et al. (1993), in which a structural fan forms in a uniform Coulomb layer above a zone of asymmetric

* Corresponding author. Present address: Department of Earth Sciences, Simon Fraser University, 8888 University Drive, Burnaby, BC, Canada V5A 1S6. Tel.: +1 604 268 7057; fax: +1 604 291 4198.
E-mail address: hdgibson@sfu.ca (H.D. Gibson).

0191-8141/$ - see front matter © 2005 Elsevier Ltd. All rights reserved.
doi:10.1016/j.jsg.2005.05.014

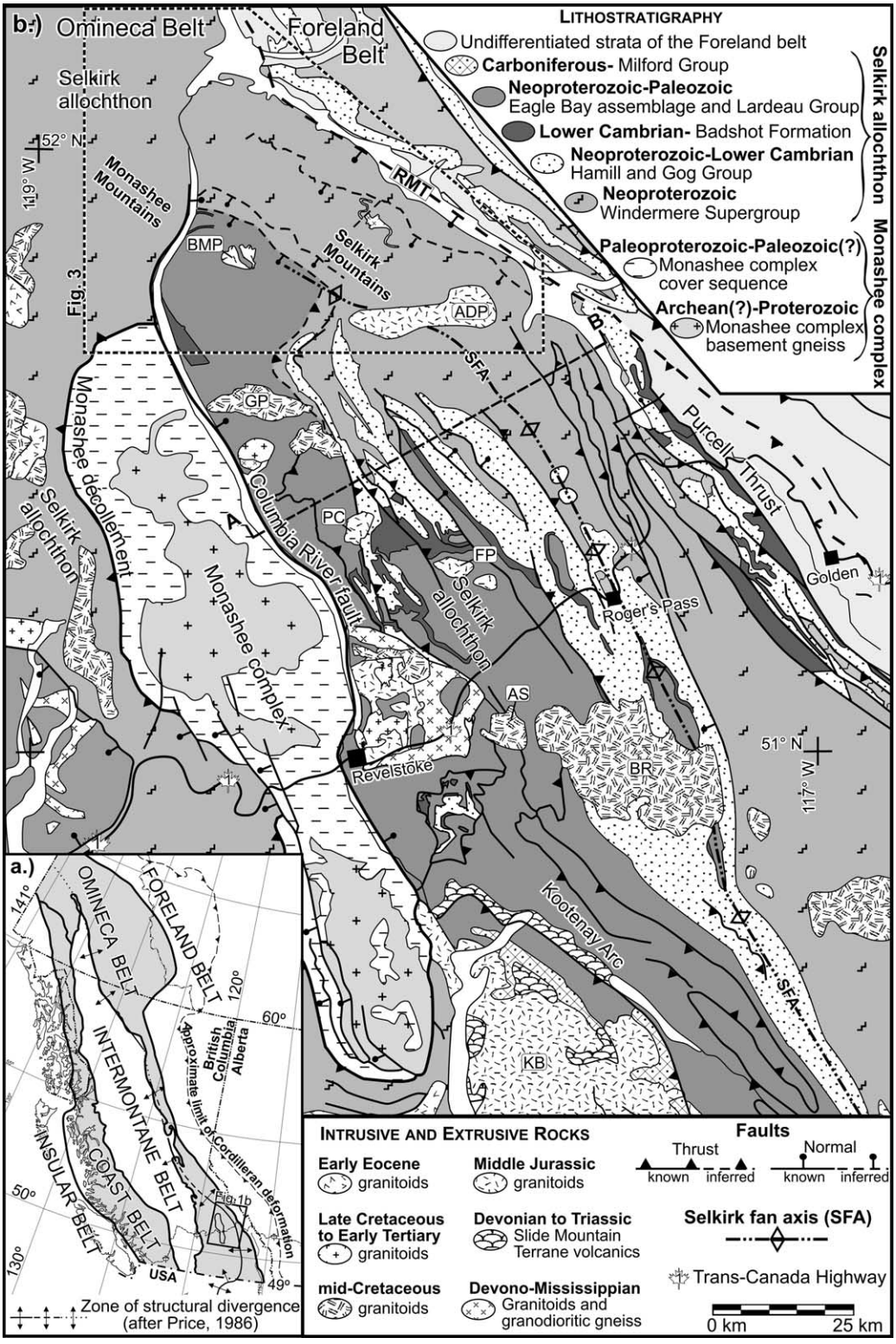

Fig. 1. (a) Morphogeologic belts of the Canadian Cordillera. (b) Tectonic assemblage map of southeastern Omineca belt (modified after Wheeler and McFeely, 1991) showing lithostratigraphy of autochthonous Monashee complex (North American basement) and overlying Selkirk allochthon. Box outlined in the top left of the figure represents the location of Fig. 3. A–B is line of section for Fig. 2a. ADP = Adamant pluton; AS = Albert stock; BMP = Bigmouth pluton; BR = Battle Range batholith; FP = Fang pluton; GP = Goldstream pluton; KB = Kuskanax batholith; PC = Pass Creek pluton. RMT = Rocky Mountain Trench.

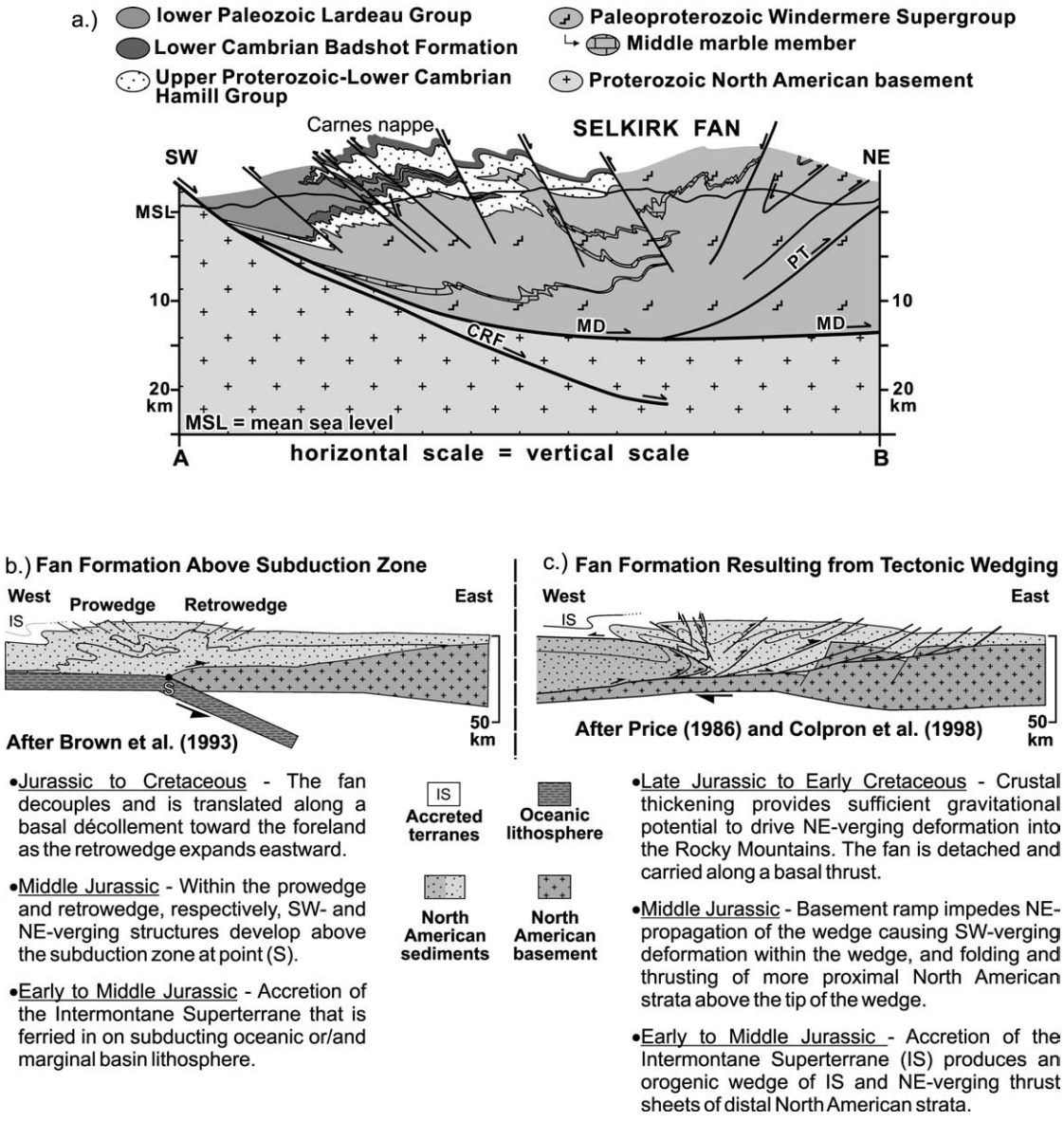

Fig. 2. (a) Generalized cross-section of the Selkirk fan for section line A–B of Fig. 1 (modified after Brown et al., 1993). Structures below ~10 km are partly constrained by Lithoprobe seismic-reflection profiles (Cook et al., 1992). CRF = Columbia River fault; MD = Monashee décollement; PT = Purcell thrust. (b) and (c) Two principal tectonic models for the formation of the Selkirk fan.

detachment and subduction of the underlying substrate (e.g. lithospheric mantle). Alternatively, Price (1986) ascribed the development of the fan to tectonic wedging of an allochthonous terrane between the cratonic basement and the overlying miogeoclinal cover. Colpron et al. (1998) revised this model, arguing that an inherited basement ramp impeded the eastward displacement of an orogenic wedge consisting, in part, of North American strata. Consequently, southwest-vergent structures were formed as the orogenic wedge was tectonically inserted eastward between more proximal strata and the cratonic basement. Once the tectonic pile attained sufficient gravitational potential, it overrode and cannibalized the ramp, resulting in the eastward propagation of northeastward-verging deformation into the Foreland belt (Fig. 2c). In both models the fan developed primarily in the Middle to Late Jurassic, constrained primarily by a limited number of meaningful U–Pb and $^{40}Ar/^{39}Ar$ ages for plutons sampled exclusively within the west side of the fan (e.g. Shaw, 1980; Brown et al., 1992; Colpron et al., 1996).

We present new U–Th–Pb isotopic data from isotope dilution thermal ionization mass spectrometry (IDTIMS) and sensitive high resolution ion microprobe (SHRIMP) analyses that provide age constraints for deformation associated with the development of the Selkirk fan. Ages for variably deformed leucocratic dikes and monzonitic–granodioritic plutons sampled across the breadth of the Selkirk fan demonstrate it is a composite of Middle to Late Jurassic (ca. 172–156 Ma) and Early to Late Cretaceous (ca. 104–81 Ma) structures.

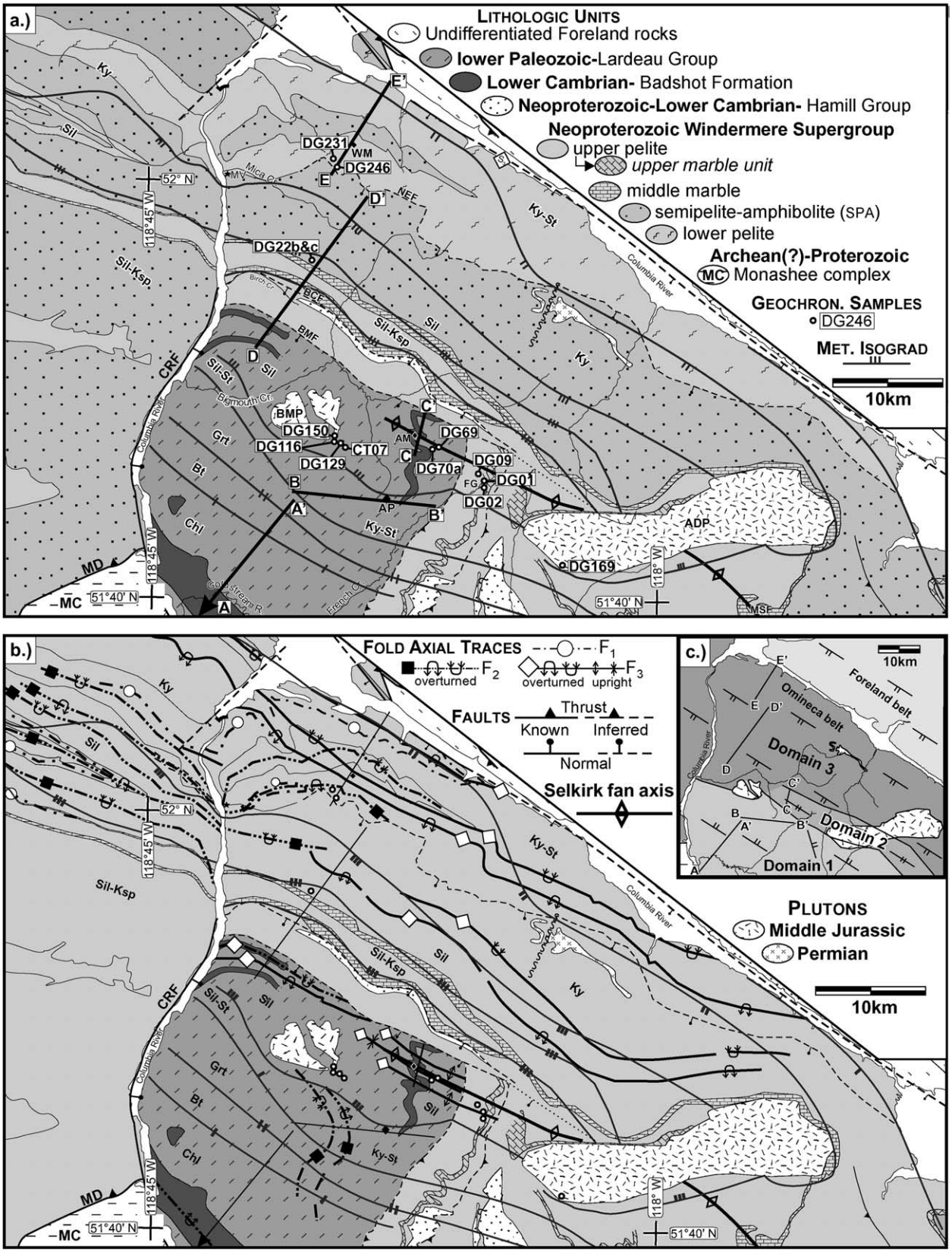

Fig. 3. Generalized geologic map of the northern Selkirk Mountains illustrating: (a) lithostratigraphy, major structures and regional metamorphic isograds, and (b) axial surface traces of F_1, F_2 and F_3. Note that Windermere Supergroup is undifferentiated in (b). Maps (a) and (b) were compiled from mapping by Brown (1991), Brown and Tippett (1978), Colpron et al. (1995), Leatherbarrow (1981), Marchildon (1999), Perkins (1983), Poulton and Simony (1980), Raeside and Simony (1983), Scammell (1993), Simony et al. (1980) and Wheeler (1965). In map (a), A–A′, B–B′, C–C′, D–D′ and E–E′ represent the lines of cross-sections

2. Geologic setting

The Late Proterozoic to Paleozoic metasedimentary and metavolcanic rocks of the northern Selkirk Mountains were originally deposited along the rifted western paleomargin of the North American craton (Gabrielse and Campbell, 1991, and references therein). During the Middle Jurassic to Paleocene these rocks were displaced northeastward ~250–300 km along a basal shear zone (Price and Mountjoy, 1970; Brown et al., 1993; Parrish, 1995) as part of the Selkirk allochthon (Read and Brown, 1981). During this time the allochthon is interpreted to have experienced protracted and diachronous internal deformation and metamorphism (Parrish, 1995). Early Tertiary normal faulting dissected and exposed all levels of the allochthon, including the Precambrian basement of the Monashee complex (Fig. 1b), a metamorphic core complex denuded by low-angle normal faults (Coney, 1980; Parrish et al., 1988).

The rocks of the northern Selkirk Mountains were subjected to at least three generations of superposed folding, and were metamorphosed at low to high grade. Bounding the eastern flank of this region is the southern Rocky Mountain trench (RMT; Fig. 1b). The trench also represents the boundary between the southern Omineca and Foreland belts. The trace of a major out-of-sequence, northeast-verging Cretaceous contractional fault, the Purcell thrust, is mapped within the trench, but is transected and obscured at the latitude of this study (~52°N, Figs. 1 and 3) by an en échelon series of down-to-the-west Tertiary normal faults (Simony et al., 1980). The western flank of the study area is partly within the hanging wall of the north- to northwest-striking, Eocene Columbia River normal fault (Read and Brown, 1981). This fault juxtaposed greenschist-facies rocks within the Selkirk Mountains against upper amphibolite-facies footwall rocks of the Monashee complex. The surface trace and magnitude of displacement of this fault disappear just south of 52°N latitude at the confluence of Birch Creek and the Columbia River (Figs. 1 and 3). North of this point, the regional northwest-trending stratigraphy, structures, and isograds are continuous across the Columbia River into the northern Monashee Mountains (e.g. Simony et al., 1980; Raeside and Simony, 1983; Scammell, 1993) (Fig. 3).

2.1. Stratigraphy

The most widespread unit in the area is a clastic turbidite sequence of the Late Proterozoic Windermere Supergroup (Wheeler, 1965; Brown et al., 1978; Perkins, 1983). It is overlain by the Eocambrian Hamill Group quartzites, the Lower Cambrian archaeocyathid-bearing marbles of the Badshot Formation, and the basinal deep-water facies carbonates, calc-silicates, metavolcanics, and schists of the Lower Paleozoic Lardeau Group. Brown et al. (1978) subdivided the lithostratigraphy of the Windermere Supergroup in the northern Selkirk Mountains into three members: the Lower Pelite, Middle Marble, and Upper Pelite. Here the same subdivisions are used, except that a distinctive Semipelite–Amphibolite (SPA) unit is considered separately, rather than as a part of the Lower Pelite member. This is consistent with subdivisions proposed by Poulton and Simony (1980) and Perkins (1983), and by workers in the northern Monashee Mountains (e.g. Simony et al., 1980; Raeside and Simony, 1983).

2.2. Structural setting

The structural style in the northern Selkirk Mountains is dominated by northwest–southeast-trending folds and faults (Fig. 3a and b). The change in vergence of these structures from southwestward to northeastward defines the geometry of the Selkirk fan (Figs. 2a and 4). Three generations of structures are described based on overprinting and geometric observations. Reference to fold and fabric generations does not necessarily imply regional timing correlations, especially across the fan axis.

2.2.1. First generation: F_1 Carnes nappe

The earliest folds, F_1, and associated axial planar foliation, S_1, are found primarily on the west flank of the fan. Here there is a km-scale, southwest-vergent, isoclinal recumbent fold termed the Carnes nappe (Brown and Lane, 1988) (Fig. 2a). Identification of shallow plunging F_1 folds and associated gently dipping axial planar S_1 foliation defined by the alignment of muscovite and biotite is complicated due to the pervasively intense overprint of F_2 folds. However, recognition of overturned stratigraphy (Read and Brown, 1979; Brown et al., 1983) interpreted as the inverted limb of the Carnes nappe (Brown and Lane, 1988; Brown, 1991), and the rare preservation of rootless isoclines and S_1 refolded by F_2 folds (Brown and Tippett, 1978; Colpron et al., 1998) provide evidence for D_1. These folds developed prior to the attainment of peak metamorphism because peak minerals and isograds are unaffected by F_1 (Wheeler, 1965; Brown and Tippett, 1978; Simony et al., 1980; Brown and Lane, 1988).

2.2.2. Second generation: F_2 folds and S_2 transposition foliation

Kilometer- to outcrop-scale, tight to isoclinal folds that are axial planar to the regional transposition fabric represent second generation structures throughout the region (see

drawn in Fig. 4. Geochronologic sample locations are also included. Abbreviations: ADP = Adamant pluton; AM = Argonaut Mountain; AP = Argonaut Pass; BMP = Bigmouth pluton; BCF = Birch Creek fault; BMF = Bigmouth fault; CRF = Columbia River fault; FG = French glacier; MV = Mica Creek village; MD = Monashee décollement; MSF = Mount Sir Sanford; NEF = Northeastern fault. Mineral abbreviations for metamorphic zones (e.g. Chl, Bt, Grt) after Kretz (1983).

Figs. 3 and 4). On both sides of the fan axis, F_2 folds and the associated S_2 transposition foliation are pervasive and dominate the structures observed at outcrop scale. F_2 hinge lines generally have a shallow plunge of ~5–25° toward the northwest or southeast. F_2 folds have highly attenuated limbs, and are typically isoclinal and recumbent, except in the fan axis where S_2 axial planes and schistosity are near-vertical. West of the fan axis, F_2 folds become increasingly overturned toward the southwest with axial planes that dip 10–20°. Conversely, F_2 folds east of the fan axis verge to the northeast, with moderate to shallow southwest-dipping S_2 axial planes and schistosity. Throughout the region, F_2 is interpreted to be synchronous with regional metamorphism (e.g. Brown and Tippett, 1978; Perkins, 1983) based on the alignment of kyanite, sillimanite, biotite and muscovite within S_2, and the preferred orientation of their long axes within the L_2 lineation. However, across the fan the same metamorphic porphyroblasts are also observed to have overgrown S_2 (this study; Brown and Tippett, 1978; Perkins, 1983). Thus, throughout the region metamorphism is interpreted to have been synchronous with, but outlasted, D_2 regardless of when D_2 developed. The implications of these observations are addressed in more detail in the Discussion section.

2.2.3. Third generation: F_3 folds, L_3 crenulations, and S_3 crenulation cleavage

Outcrop- to km-scale third generation folds (F_3) are found primarily east of the fan axis where they refold F_2 and S_2 structures. Northeast-verging F_3 folds are generally more upright than F_2, and have moderate-dipping axial planes (~40–80°) that tend to be less steeply inclined (~15–40°) adjacent to the Rocky Mountain Trench. The F_3 fold style is typically Class 1B or Class 1C, with a close to tight geometry. Development of F_3 is interpreted to have occurred during the late stages of, and/or following, regional metamorphism (e.g. Brown and Tippett, 1978; Simony et al., 1980; Perkins, 1983). These folds are generally coaxial with F_2, which resulted in Type-3 interference patterns. West of the fan axis, D_3 is less well developed; it is interpreted to be present mainly as near-upright, shallow-plunging L_3 crenulations and S_3 crenulation cleavage that transect the S_2 transposition foliation at a high angle (Brown and Tippett, 1978).

2.3. Metamorphism

In the study area, sillimanite- and sillimanite–K-feldspar-grade rocks core the Selkirk fan, and are flanked on either side by progressively lower grade assemblages (Fig. 3). A set of northwest-trending regional isograds has been mapped based on the appearance or disappearance of biotite, muscovite, garnet, staurolite, kyanite, and sillimanite (Wheeler, 1965; Campbell, 1968; Ghent et al., 1977; Simony et al., 1980; Leatherbarrow, 1981). In general, the isograds trend northwest–southeast parallel to the structural grain of the region, except where they crosscut the trace of F_2 structures south of the Bigmouth pluton (Fig. 3b). The lowest grade assemblages in the chlorite zone are located on the west flank of the fan in the immediate hanging wall of the Columbia River fault (Fig. 3). The metamorphic grade increases eastward until the sillimanite–K-feldspar zone is encountered near the fan axis, and then decreases to the northeast where staurolite–kyanite assemblages occur adjacent to the Rocky Mountain Trench.

3. Previous timing constraints for deformation

3.1. Southwest-verging structures: D_1 and D_2

In regions adjacent to the northern Selkirk Mountains, Murphy et al. (1995) constrained the age of southwest-verging F_1 and F_2 folds to be ca. 185–174 Ma. The older age limit is based, in part, on the 187–185 Ma Hall Formation that is located within the hanging wall of the Stubbs thrust, which was subsequently folded by F_1. The younger age limit is based on the 174 Ma Hobson Lake pluton, which is interpreted to truncate all southwest-vergent D_1 and D_2 structures in the Cariboo Mountains to the north (Gerasimoff, 1988).

Prior to this study, meaningful age constraints for southwest-verging deformation and associated metamorphism were primarily provided by U–Pb analyses of zircon and titanite from Middle Jurassic plutons located within the western flank of the fan. Shaw (1980) analyzed zircon from the southwestern part of the Adamant pluton (Fig. 3). He concluded that the 169 ± 4 Ma U–Pb age represented the time of metamorphic zircon growth during D_2, rather than pluton emplacement, because the zircon could be found only in the outer, hydrated zone of the pluton. U–Pb analyses of zircon and titanite by Brown et al. (1992) produced an age of ca. 168 Ma for the Fang and Pass Creek plutons (Fig. 1b), which were interpreted to post-date the development of southwest-verging structures and regional metamorphism. Thus, in the northern Selkirk Mountains, D_1, D_2, and regional metamorphism were interpreted to have occurred prior to and possibly during 169 Ma, but no later than 168 Ma.

However, Colpron et al. (1996) argued that the earliest deformation in the Selkirk Mountains coincided with the initial obduction of the Intermontane Superterrane and development of ca. 187–173 Ma northeast-verging folds and faults (Colpron et al., 1996, and references therein). Subsequent development of southwest-vergent folds and faults occurred between ca. 173 and 168 Ma based, in part, on $^{40}Ar/^{39}Ar$ cooling ages of four plutons, including the Fang pluton, interpreted to have been emplaced late synkinematic with respect to southwest-vergent deformation. Using thermochronometric and thermobarometric data from these plutons, Colpron et al. (1996) also showed

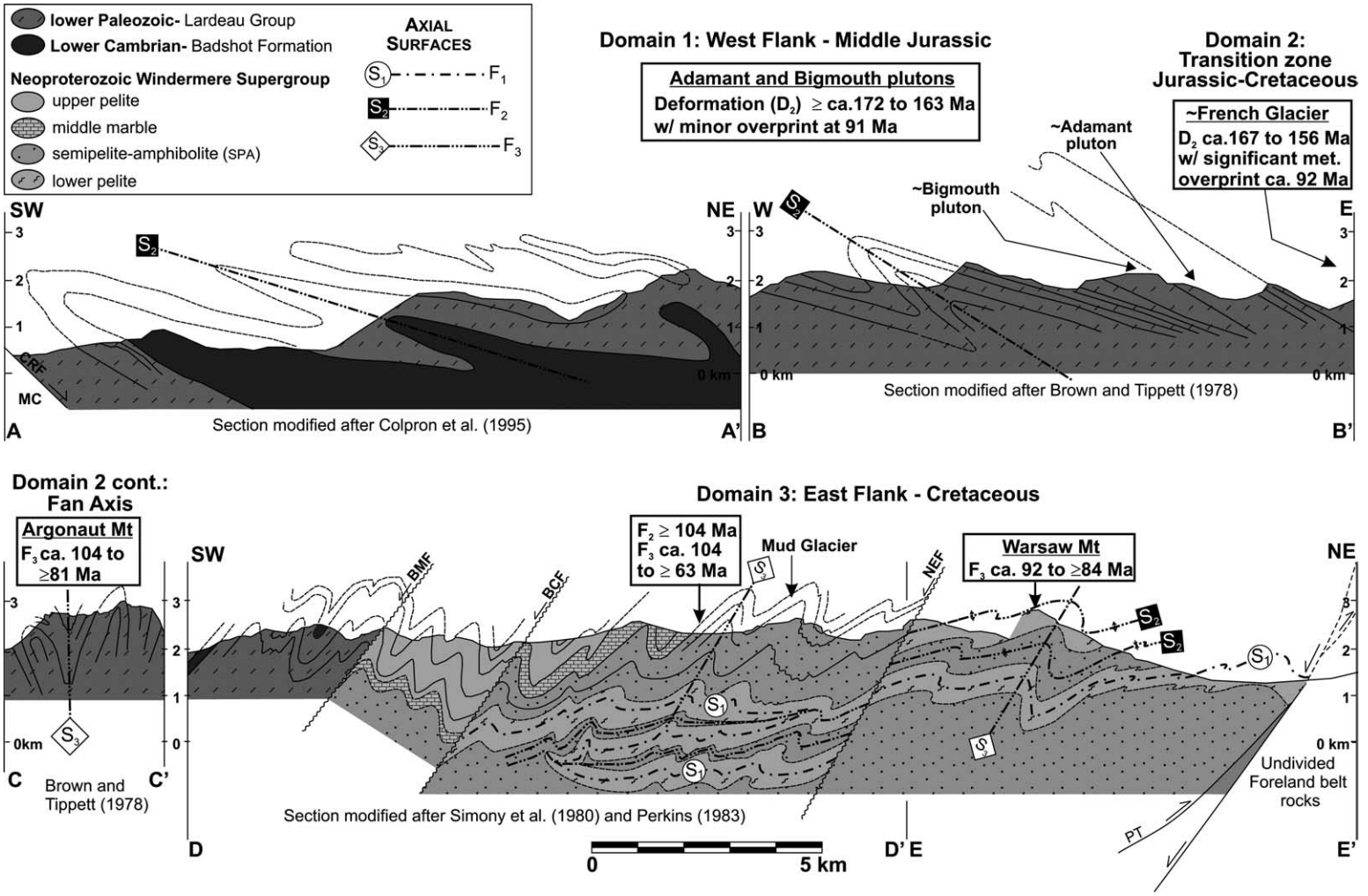

Fig. 4. Composite structural cross-section that transects the study area, illustrating the geometry of the fan, modified after Brown and Tippett (1978), Colpron et al. (1995), Perkins (1983) and Simony et al. (1980). Section lines are located in Fig. 3. U–Th–Pb geochronologic age constraints for the time of deformation and their approximate locations have been projected along strike into the line of section.

that there was at least 10 km of exhumation during development of southwest-verging structures.

In the study area, Marchildon (1999) interpreted the Bigmouth pluton and surrounding country rocks to have been affected by two metamorphic events, M_1 and M_2, separated by an intervening period of decompression. The development of the transposition foliation (S_T) was interpreted to have been a protracted process that began prior to M_1 and continued through M_2. Pluton intrusion was interpreted to be coeval with the M_1 metamorphism, at a depth >20 km based on the presence of magmatic epidote (see Zen and Hammarstrom, 1984). A linear regression through discordant IDTIMS zircon data produced a lower intercept age of 157 ± 3 Ma, interpreted to constrain pluton emplacement and M_1, but post-dating the initiation of the transposition event. Two fractions of titanite analyzed by Marchildon gave $^{206}Pb/^{238}U$ ages of 140.5 ± 0.8 Ma and 137.4 ± 1.4 Ma with normal discordance of ~6–16%. The titanite crystals were interpreted to have been reset during M_2 following post-M_1 decompression, before the end of the transposition event. Thus, S_T was considered to be older than 157 Ma, but continued to develop after 137 Ma.

Lastly, U–Pb analyses of zircon from the Goldstream pluton (Logan and Friedman, 1997) and the Albert stock (Crowley and Brown, 1994) both yielded an age of 104 Ma. Both intrusive bodies are situated within the west flank of the fan (Fig. 1b) where they truncate all structures in the country rock, contain foliated xenoliths of the host bedrock, and are surrounded by a contact aureole that overprints the regional metamorphic assemblage. Thus, development of southwest-vergent structures and metamorphism in the western flank occurred prior to 104 Ma.

3.2. Northeast-verging structures: D_2 and D_3

Relative timing constraints for northeast-verging structures in the northern Selkirk Mountains were proposed by Brown and Tippett (1978) and Brown et al. (1992). They inferred that the development of F_2 was closely related to regional metamorphism that predated the emplacement of the Middle Jurassic Fang and Pass Creek plutons (ca. 168 Ma). However, the deflection of F_2 structures around these igneous bodies was interpreted to be associated with F_3 (Brown et al., 1992). Thus, F_3 was interpreted to be post-Middle Jurassic. Colpron et al. (1998) suggested that the formation of northeast-vergent structures in the Dogtooth Range east of the fan axis coincided with the initial Late Jurassic tectonic loading of the foreland basin, marked by the Kimmeridgian age deposition of the Passage beds of the Fernie Group (Price, 1994).

Prior to this study, the only absolute time constraints for northeast-verging structures in the northern Selkirk Mountains came from Crowley et al. (2000). IDTIMS analyses of monazite and zircon from pre- to syn- and post-tectonic leucocratic dikes collected along Highway 23 near Mica Creek Village (MV; Fig. 3a) suggest fold (F_{2-3}) and foliation (S_{1-2}) development to be ca. 122–58 Ma (Crowley et al., 2000). These ages agree well with those provided by other studies to the west and northwest in the northern Monashee Mountains (Sevigny et al., 1989, 1990; Scammell, 1993; Digel et al., 1998). However, Crowley et al. (2000) also produced ages between ca. 170 and 58 Ma for northeast-verging D_2 structures and metamorphic assemblages in the northern Monashee Mountains. The implications of these data are considered below.

4. U–Th–Pb geochronology: new timing constraints on deformation

Zircon and monazite U–Th–Pb isotopic data are reported for 14 samples that include variably deformed leucosome, leucogranitic dikes, and plutons. The data are presented in concordia diagrams (Figs. 5–15) and summarized on a regional cross-section (Fig. 4). The complete IDTIMS and SHRIMP analytical data sets are provided as an electronic supplement (see 'Electronic Supplements (ES)' on the journal homepage: http//www.elsevier.com/locate/jsg).

The study area has been broadly divided into three domains (Figs. 3c and 4) based on their lithostratigraphic, structural, metamorphic and geochronologic elements. Domain 1 is in the west flank of the fan where southwest-verging F_2 structures dominate. This domain is interpreted to represent the highest structural level[1] in the study area, comprising primarily rocks of the Lardeau Group and Badshot Formation that were metamorphosed at chlorite to sillimanite grade, and intruded by Middle Jurassic plutons. Deformation and metamorphism are constrained to be Middle to Late Jurassic (ca. 172–156 Ma; this study), with a minor overprint at ca. 91 Ma (Fig. 6c and d). Domain 2 occupies the zone where the trace of the fan axis is mapped (Fig. 3), and is cored by sillimanite-grade rocks of the Windermere Supergroup, with near-vertical structures that generally strike to the northwest or southeast. Domain 2 is termed the 'Transition Zone' because the isotopic data indicate that Middle Jurassic structures were substantially overprinted during the mid- to Late Cretaceous (ca. 104–81 Ma). Domain 3 is in the eastern flank of the fan where northeast-vergent folds (F_2 and F_3) and a transposition foliation (S_2) dominate at all scales of observation. The east flank is composed of Windermere Supergroup rocks that change from sillimanite–K-feldspar grade near the fan axis to kyanite–staurolite grade adjacent to the Rocky Mountain Trench. In Domain 3, age constraints range from Early Cretaceous to Early Tertiary (ca. 144–63 Ma; this study; Gibson, 2003).

[1] All references to 'structural or crustal level' correspond to the paleo-level in the Jurassic and/or Cretaceous.

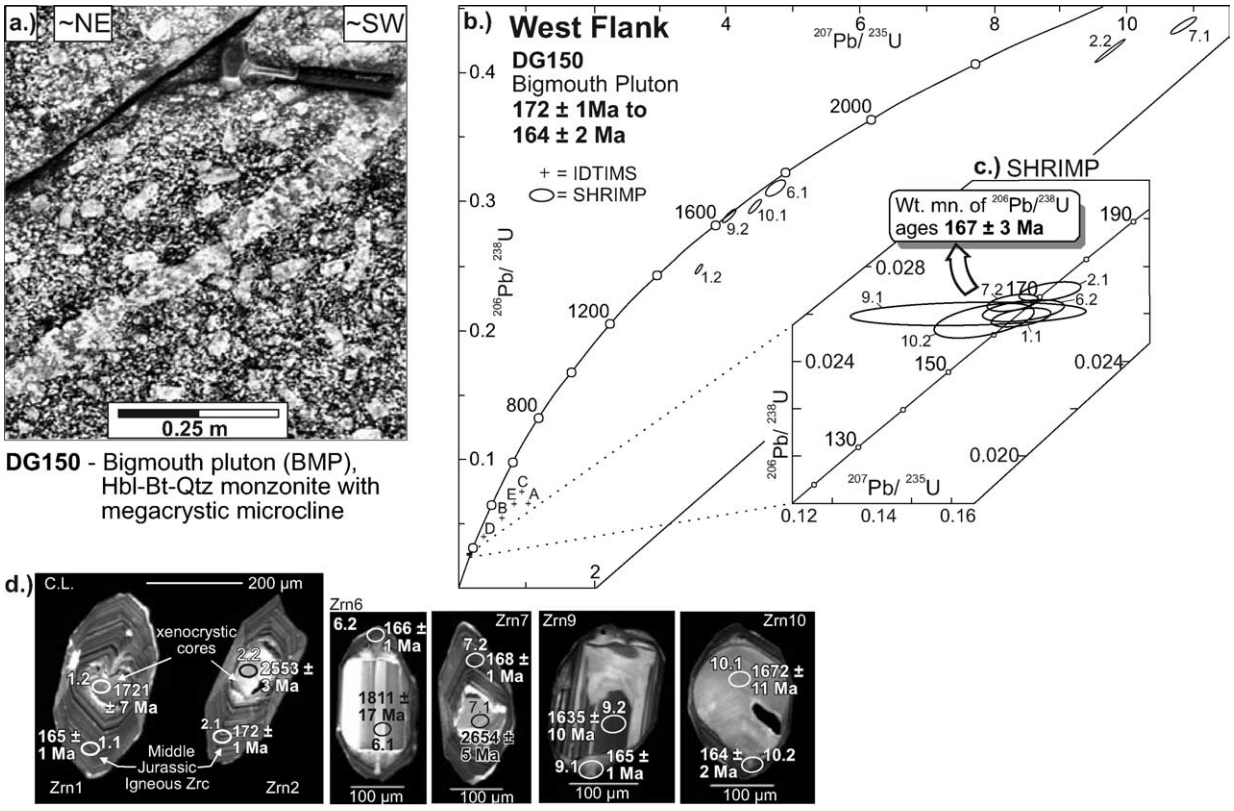

Fig. 5. (a)–(d) Sample DG150. (a) Outcrop photo. (b) IDTIMS and (c) SHRIMP U–Pb concordia plots. (d) CL images of zircon grains with spot locations and ages for SHRIMP analyses.

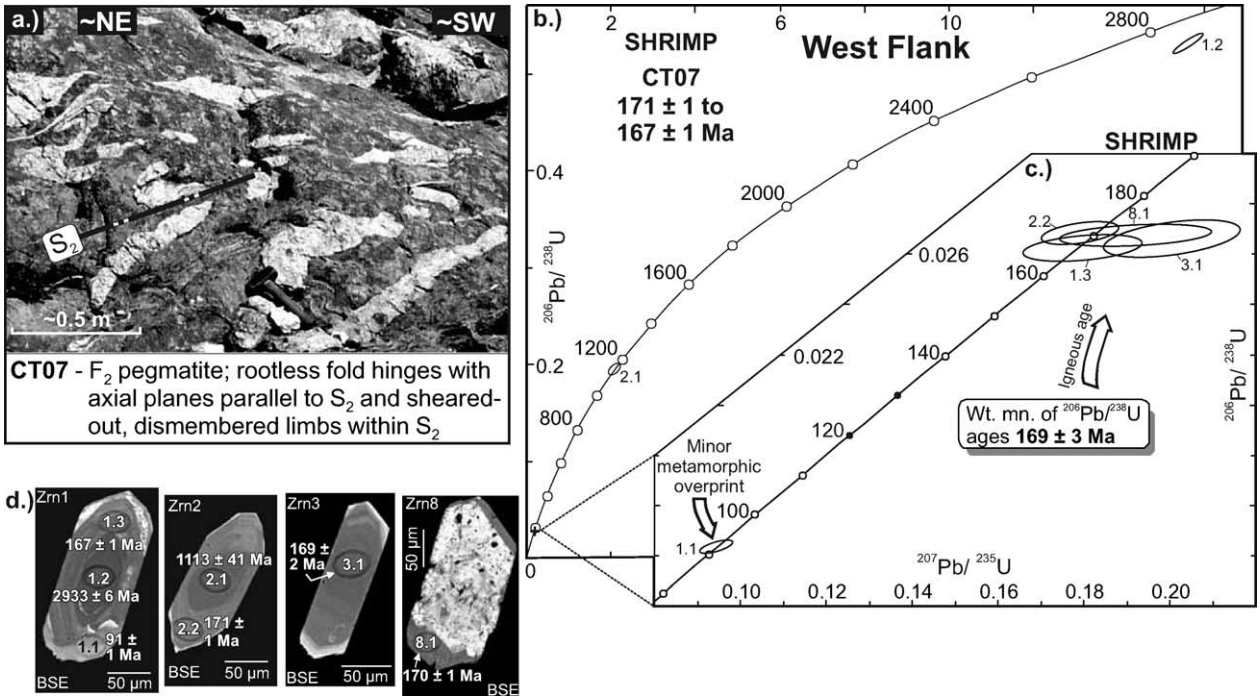

Fig. 6. (a)–(d) Sample CT07. (a) Outcrop photo. (b) U–Pb concordia plot for all SHRIMP analyses. (c) Blow up of concordia diagram showing the analyses that provide the igneous age of CT07 (169 Ma) and the overprint at 91 Ma. (d) CL images of the zircon and locations of the SHRIMP spots and their ages.

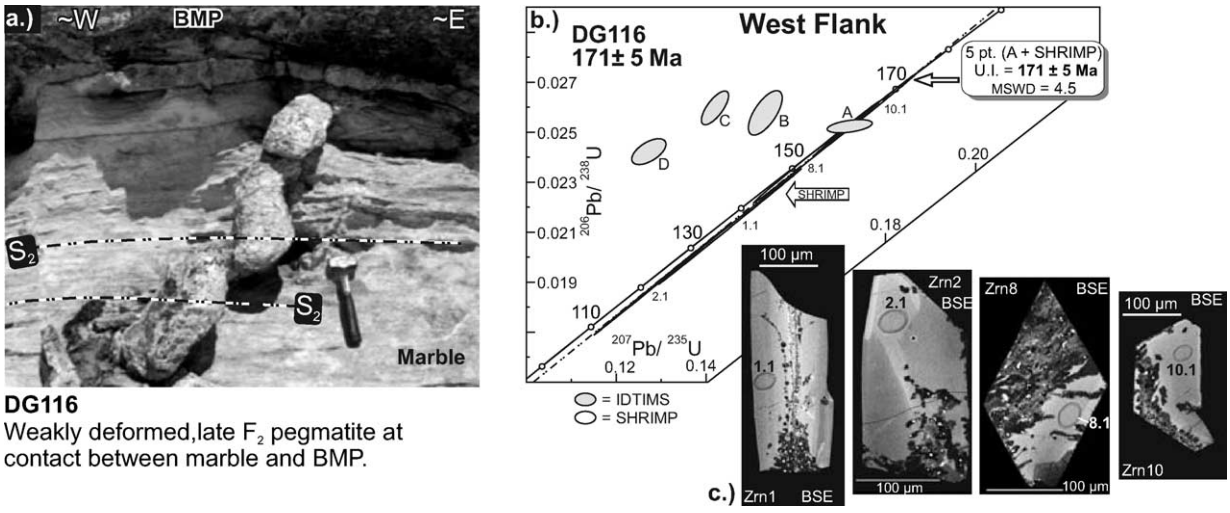

Fig. 7. (a)–(c) Sample DG116. (a) Outcrop photo. (b) IDTIMS and SHRIMP U–Pb concordia plots accompanied by (c) BSE images of the zircon grains analyzed by SHRIMP with the spot locations and ages.

4.1. Analytical methods

Geochronologic data were acquired using U–Pb IDTIMS and U–Th–Pb SHRIMP methods, accompanied by back-scattered electron (BSE) and cathodoluminescence (CL) imaging, and high-resolution X-ray compositional maps of dated minerals. Integration of these techniques was necessary to resolve complexities such as multiple age domains within single crystals and young monazite with Th disequilibrium (see Schärer, 1984). BSE and CL images were obtained using a Cambridge Instruments S360 scanning electron microscope. Chemical maps of Y, Th, and U of strategically selected monazite crystals were made using a Cameca SX-50 electron microprobe at the University of Massachusetts (see Williams et al. (1999) for procedural details). The use of chemical maps to guide SHRIMP II analyses of monazite proved to be very effective for elucidating age domains within the analyzed crystals (see also Gibson et al., 2004).

U–Pb IDTIMS geochronology at Carleton University followed procedures outlined by Parrish et al. (1987). All zircon grains, with the exception of some <74 µm

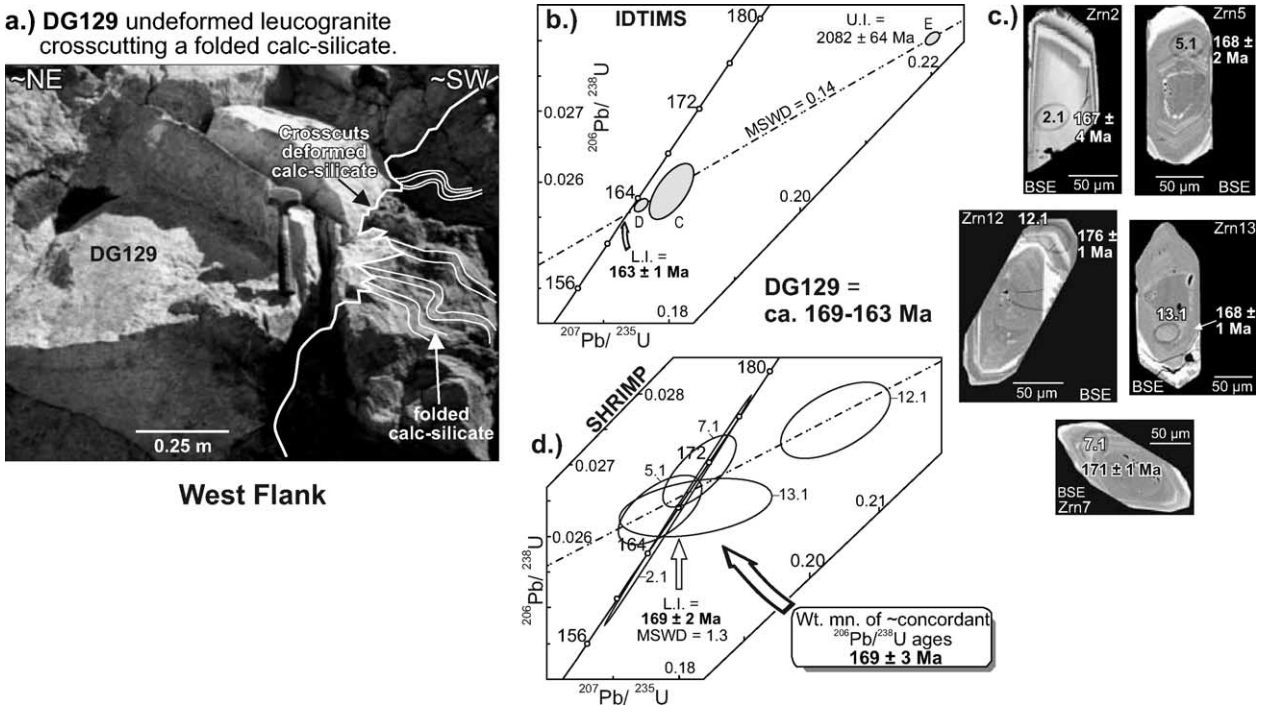

Fig. 8. (a)–(d) Sample DG129. (a) Outcrop photo. (b) IDTIMS U–Pb concordia plot. (c) BSE images of the zircon grains analyzed by SHRIMP with the spot locations and ages. (d) SHRIMP U–Pb concordia plot.

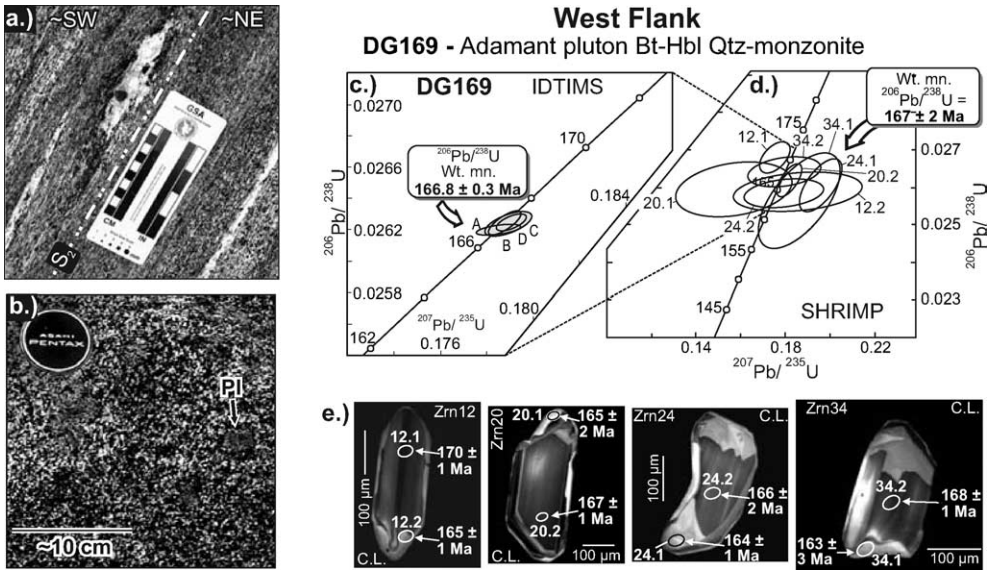

Fig. 9. (a)–(e) (a) Outcrop photo of highly strained Adamant pluton near its eastern margin. The foliation is parallel to S_2 within the host country rock. (b) Outcrop photo of DG169, located near the western margin of the Adamant pluton, showing very little evidence of strain. (c) IDTIMS and (d) SHRIMP U–Pb concordia plots for DG169 accompanied by (e) CL images of zircon and spot locations and ages for SHRIMP analyses.

fractions, were abraded according to Krogh (1982). Teflon® microcapsules (Parrish, 1987) were used for mineral dissolution with a mixed ^{233}U–^{235}U–^{205}Pb tracer (Parrish and Krogh, 1987). Ion exchange column chemistry (Parrish et al., 1987) facilitated U–Pb element separation. Decay constants used are those recommended by Steiger and Jäger (1977). U–Pb isotopes were analyzed using a multicollector mass spectrometer (MAT 261, as described by Roddick et al.

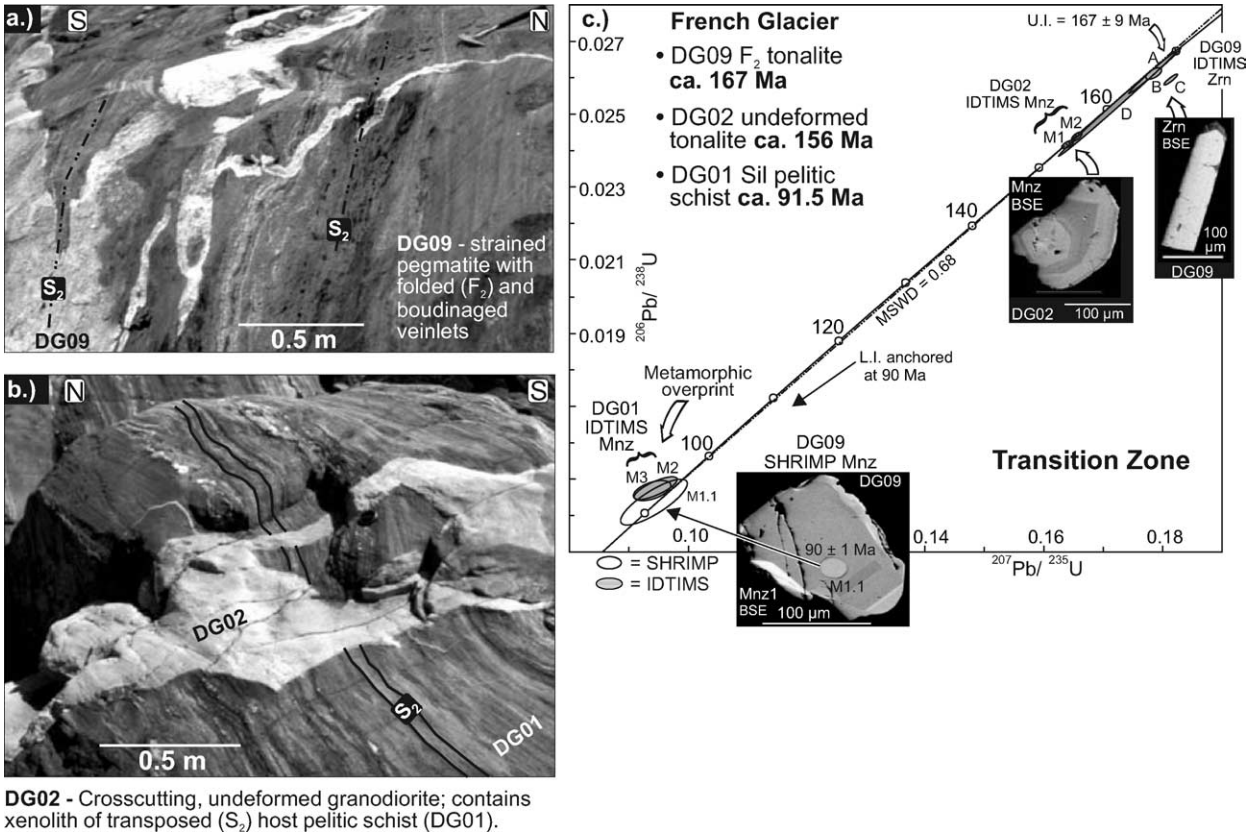

Fig. 10. (a)–(c) Outcrop photos for samples (a) DG09 and (b) DG02. (c) IDTIMS and SHRIMP U–Pb concordia plot for DG01, DG02 and DG09, accompanied by BSE images of representative zircon and monazite from DG02 and DG09. Note the SHRIMP spot for the monazite belonging to DG09 (lower left part of the concordia plot) that provides a Late Cretaceous age (90 ± 1 Ma), is interpreted to be the time of a metamorphic overprint.

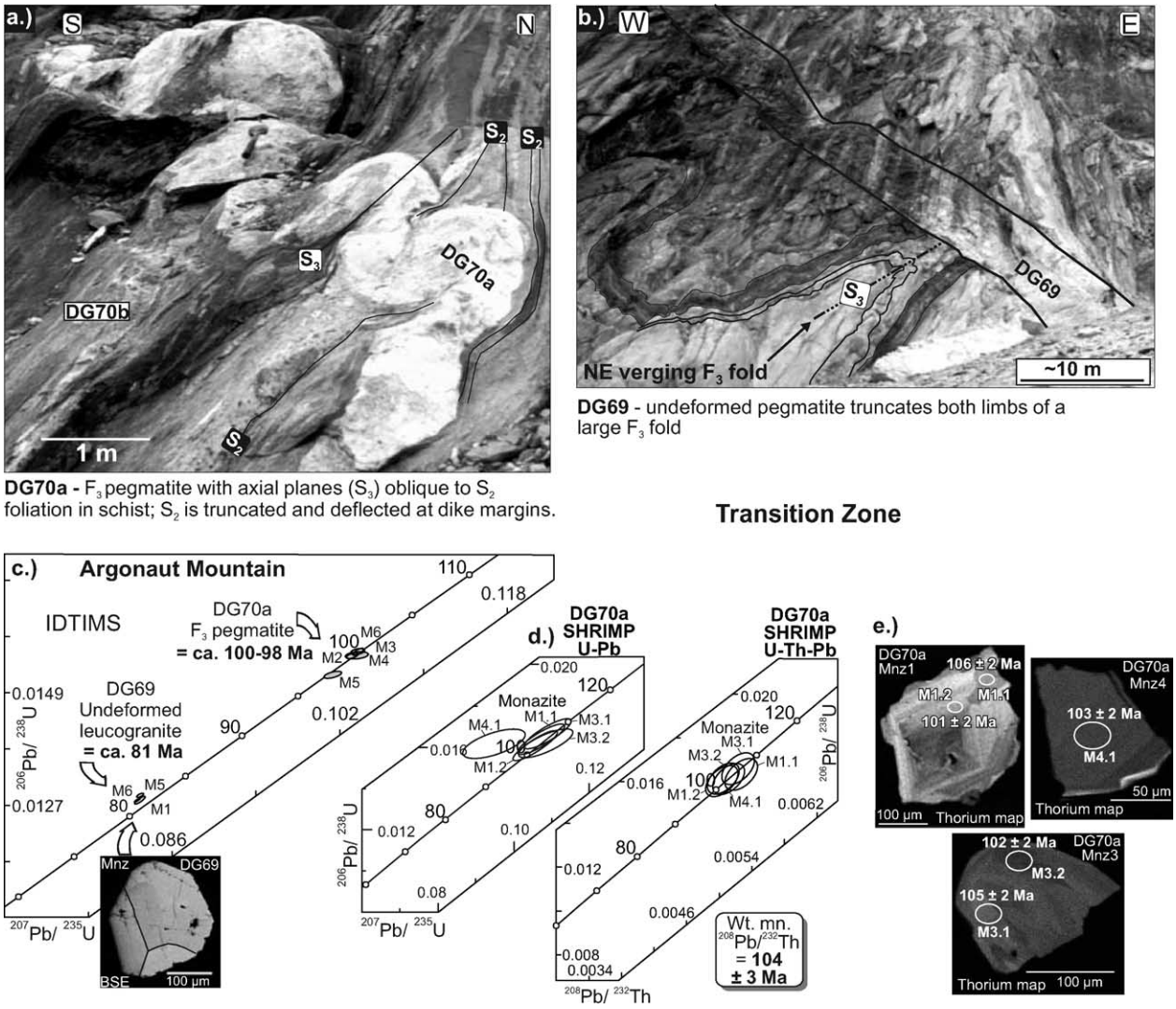

Fig. 11. (a)–(e) Outcrop photos for samples (a) DG70a (and DG70b) and (b) DG69. (c) IDTIMS concordia plot for DG70a and DG69, accompanied by BSE image of a monazite from DG69 (note: sector zoning highlighted by line drawing). (d) SHRIMP U–Pb and U–Th–Pb concordia plots for DG70a. (e) Thorium chemical maps of monazite from DG70a that were analyzed by SHRIMP with the spot locations and ages.

(1987)), and estimation of errors was based on numerical error propagation (Roddick, 1987).

SHRIMP analyses of monazite and zircon grains in a polished mount were carried out at the Geological Survey of Canada in Ottawa according to the methods outlined by Stern (1997), Stern and Sanborn (1998) and Stern and Berman (2000). Errors assigned to SHRIMP U–Th–Pb ages were determined using numerical propagation of all known sources of error (see Stern, 1997; Stern and Berman, 2000). The ^{204}Pb correction can impart significant error on the calculated age for SHRIMP data due to extremely low ^{204}Pb counts (see Stern, 1997). The propagation of the associated statistical error usually has the most impact on the ^{207}Pb/^{235}U age, because of low ^{207}Pb counts in relatively young minerals (i.e. Jurassic–Tertiary). This can cause an 'artificial' disagreement between the calculated ^{207}Pb/^{235}U age and those calculated using the other isotopic systems. Thus, the isotopic systems for monazite and zircon that include the highest Pb counts, the ^{208}Pb/^{232}Th and ^{206}Pb/^{238}U chronometers, respectively, are considered most accurate and are used when quoting SHRIMP ages in the text and figures unless otherwise noted.

4.2. Guidelines for age interpretations

The IDTIMS data in many of the samples yield an age range of a few million years or more, well outside analytical uncertainty, which is attributed to the presence of two or more age domains within the analyzed monazite or zircon. Causes for this include partial recrystallization and/or secondary growth, and inherited xenocrystic cores in zircon of variable age that make interpretation of linear regressions difficult or impossible. Additional complexities consist of crystal alteration due to metamictization and/or hydrothermal fluids, and unsupported ^{206}Pb in monazite from the incorporation of excess ^{230}Th upon crystallization (Schärer,

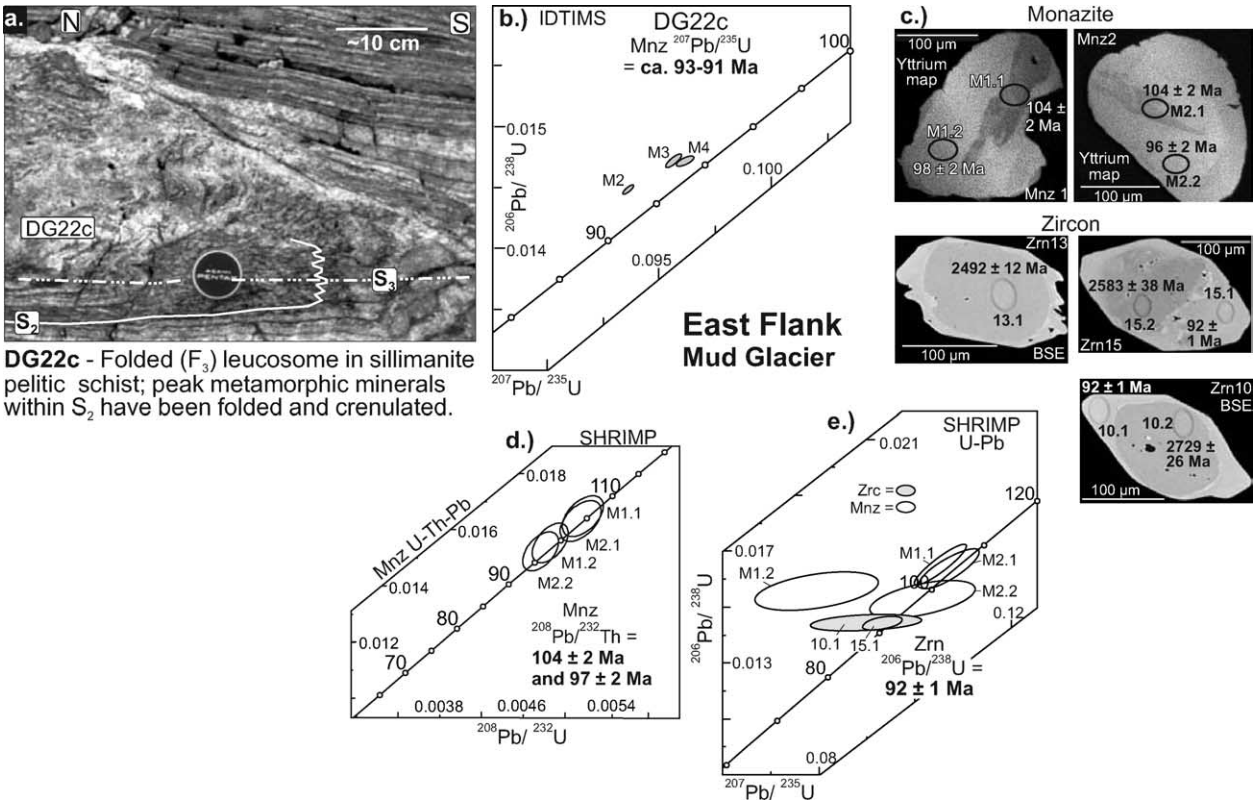

Fig. 12. (a)–(e) Sample DG22c. (a) Outcrop photo. (b) IDTIMS U–Pb concordia plot for monazite data. (c) Yttrium maps for monazite and BSE images of the zircon analyzed by SHRIMP with the spot locations and ages. (d) SHRIMP U–Th–Pb concordia plot for the monazite data, and (e) U–Pb concordia plot for both the monazite and zircon data.

1984) that increased the $^{206}Pb/^{238}U$ ages. Linear regressions through discordant IDTIMS monazite data are therefore considered unreliable because intercepts may be offset at either end if there is a component of unsupported ^{206}Pb. The correction prescribed by Schärer (1984) for unsupported ^{206}Pb in igneous monazite has not been applied because it is not considered appropriate for the monazite grains in this study. For instance, chemical maps, BSE images, and SHRIMP analyses revealed that many monazite grains have variable degrees of secondary growth and/or recrystallization (see Figs. 12 and 14). Parrish (1990) concluded that it is impossible to determine the Th/U ratios of the medium that facilitated metamorphic monazite growth-recrystallization, which is necessary to implement Schärer's correction. Furthermore, most of the IDTIMS monazite data are supplemented by SHRIMP analyses that provide $^{208}Pb/^{232}Th$ data, which are considered to be unaffected by isotopic disequilibrium. For IDTIMS data not

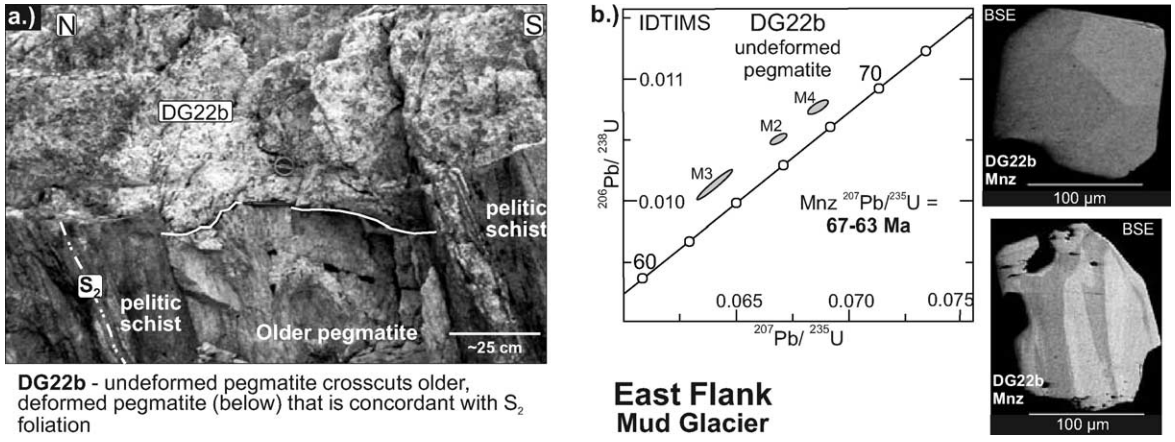

Fig. 13. (a) and (b) Sample DG22b. (a) Outcrop photo. (b) IDTIMS U–Pb concordia plot of monazite data accompanied by representative BSE images of monazite from DG22b.

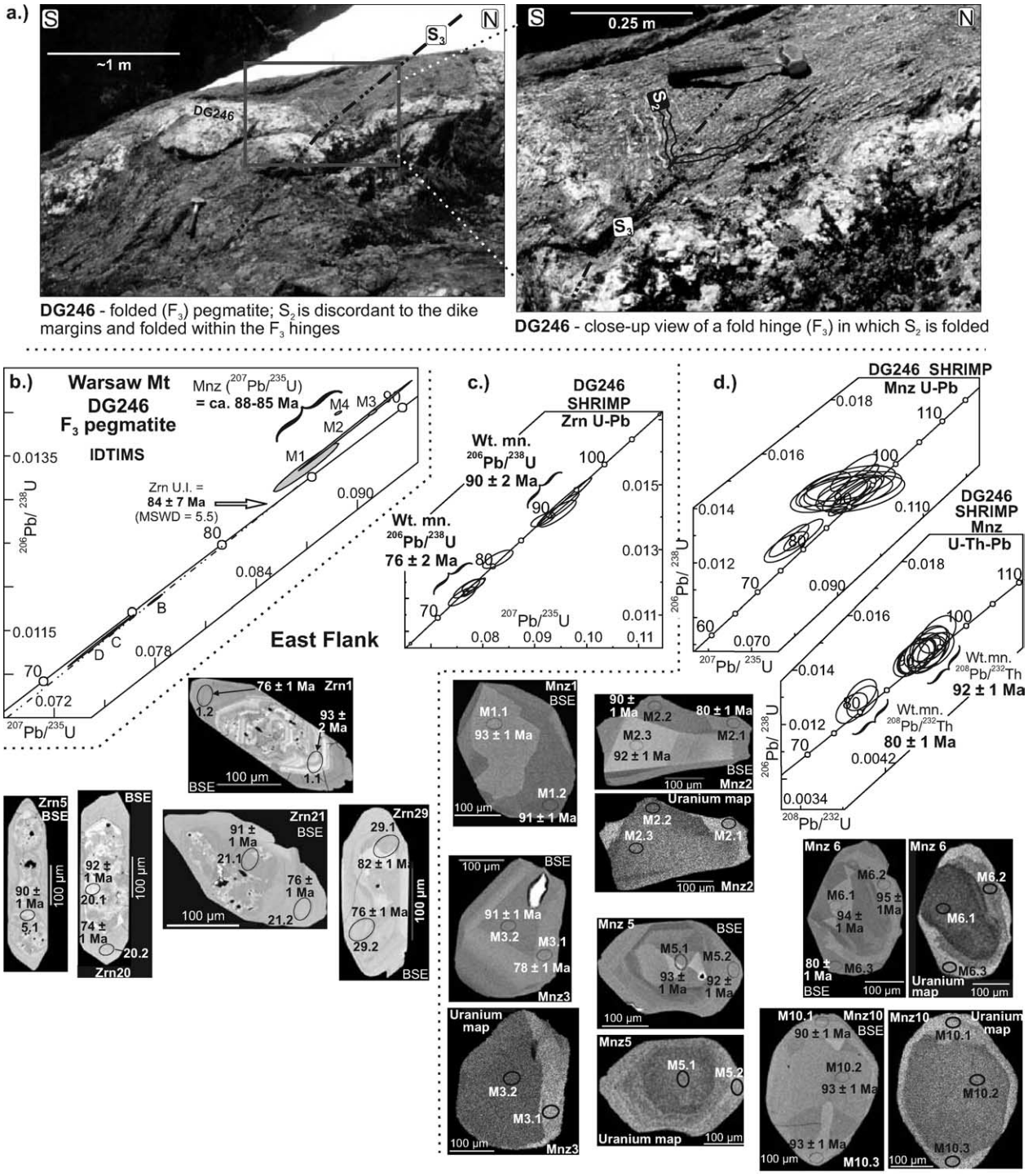

Fig. 14. (a)–(d) Sample DG246. (a) Outcrop photos of DG246. (b) IDTIMS U–Pb concordia plot of monazite and zircon data. (c) SHRIMP U–Pb concordia plot of zircon data accompanied by BSE images of the zircon analyzed with spot locations and ages. (d) SHRIMP U–Pb and U–Th–Pb concordia plots of monazite data accompanied by BSE images and Uranium maps of the monazite analyzed with spot locations and ages.

accompanied by SHRIMP analyses, it is assumed that the $^{207}Pb/^{235}U$ chronometer, also unaffected by ^{230}Th disequilibrium, best approximates the time of monazite crystallization (Schärer, 1984).

Lastly, diffusive Pb loss is considered unlikely for either zircon or monazite under most geologic conditions. Based on experimentally determined diffusion parameters, Cherniak and Watson (2000) and Cherniak et al. (2002) concluded that the mean closure temperature (see Dodson, 1973) for both zircon and monazite of typical size (10–100 µm) is in excess of 900 °C. Moreover, many in situ studies have also concluded that these minerals are highly

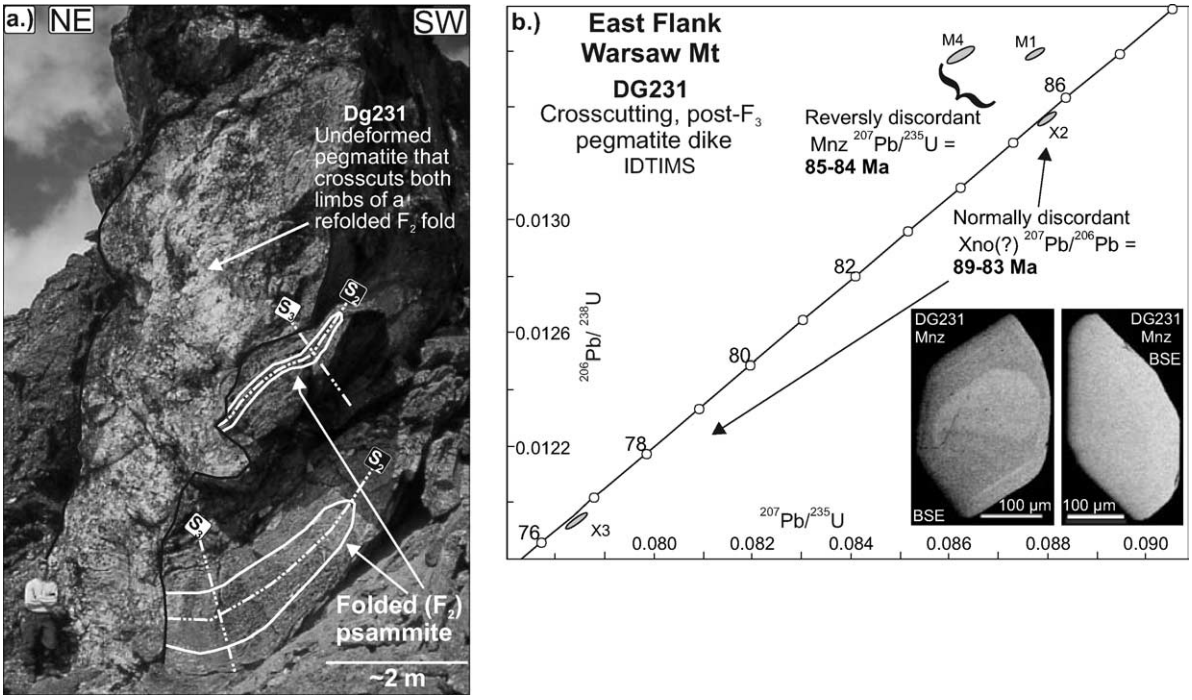

Fig. 15. (a) and (b) Sample DG231. (a) Outcrop photo. (b) IDTIMS U–Pb concordia plot of monazite and xenotime data accompanied by representative BSE images of monazite from DG231.

resistant to thermally induced volume diffusion, even during granulite facies metamorphism (e.g. DeWolf et al., 1993; Zhu et al., 1997; Braun et al., 1998; Cocherie et al., 1998; Crowley and Ghent, 1999; Zhu and O' Nions, 1999; Foster et al., 2002). Thus, a spread in ages for a given sample is attributed to either multiple intracrystalline age domains in monazite and/or zircon (e.g. inherited older cores, partial recrystallization, overgrowth), or recent Pb loss in metamict zircon.

4.3. Isotopic data and age interpretations

A summary of the ages, locations, hand sample and thin section descriptions, and geologic relationships is given in Table 1.

4.3.1. Domain 1: western flank

4.3.1.1. DG150—Bigmouth pluton (IDTIMS and SHRIMP). The Bigmouth pluton is a weakly deformed to undeformed coarse-grained hornblende–biotite–quartz monzonite to granite intrusion (Fig. 5a). Mapping near the southeast contact shows that the Bigmouth pluton is a ~1-km-thick laccolith whose lower contact dips shallowly north. The base of the pluton is generally in contact with marble and calcareous pelite. The upper contact was interpreted by mapping roof pendants of calcareous schist and marble along ridge tops. The pluton appears to truncate regional D_2 structures, and xenoliths of foliated (S_2) country rock are found near the contact, suggesting the main phase of transposition pre-dated the emplacement of the pluton. Weakly folded dikes and veinlets extending away from the contact suggest some strain following pluton emplacement (see DG116, Fig. 7).

Both IDTIMS and SHRIMP analyses were carried out on clear, euhedral zircon. Optically, some of the zircon grains appeared to have cores; thus, one IDTIMS fraction, D, consisted only of tips to minimize the effect of the inherited cores. All IDTIMS fractions are normally discordant with significant scatter (Fig. 5b) and highly variable $^{207}Pb/^{206}Pb$ ages, ca. 1956–950 Ma (ES Table 1). This precluded using linear regression to determine an igneous age for the pluton, and brought into question the age assigned by Marchildon (1999) based on linear regression of similarly dispersed data. SHRIMP analysis of zircon cores displayed by CL clarified the inheritance problem; six spots on cores of six crystals produced Archean and Early Proterozoic ages, ca. 2650–1655 Ma (Fig. 5b and d; ES Table 2). Conversely, six spots targeted in domains of pristine oscillatory zoning that surround the cores and are interpreted to represent igneous growth (see Vavra, 1990; Pidgeon, 1992; Hanchar and Miller, 1993) produced $^{206}Pb/^{238}U$ ages between 172 and 164 Ma. The analyses overlap concordia within error (Fig. 5c), and have variable discordance that is likely attributable to the imprecision of the $^{207}Pb/^{235}U$ ratio due to low ^{207}Pb counts. Thus, the $^{206}Pb/^{238}U$ SHRIMP weighted mean age of 167 ± 3 Ma is interpreted as the crystallization age of the Bigmouth pluton, and the age assigned by Marchildon (1999), 157 ± 3 Ma, is considered too young. Pluton emplacement at 167 ± 3 Ma post-dated most of the

Table 1
Summary of new U–Th–Pb age constraints for deformation in the northern Selkirk Mountains, British Columbia[a]

Sample	Lithology[b]	Mineralogy[c]	Texture/fabric/structural interpretation	Interpreted age[d]	Location (UTM)
Domain 1: West flank of fan—Bigmouth Pluton (BMP) area					
DG150 BMP	Kfs-megacrystic, Hbl-Bt bearing, Qtz-monzonite	Hbl, Bt, Kfs, Pl, Qtz, Ep, Ttn	Coarse grained; weak foliation (flow banding?) of aligned Kfs-megacrysts, Hbl, and Bt; xenoliths of wall rock containing S_2 entrained near margin	Igneous Zrn ca. 172–164 Ma; wt. mn. = 167 ± 3 Ma; interpreted to constrain latest stages of deformation in the area	E 402125, N 5739400, 2370 m
CT07	Pegmatite dike	Bt, Ms, Kfs, Pl, Qtz, Cal	Intensely strained dike, with rootless fold hinges, dismembered limbs, and axial planes parallel to S_2	Igneous Zrn ca. 171–167 Ma; Wt. mn. = 169 ± 3 Ma; Pre- to syn-D_2	E 402750, N 5738310, 2410 m
DG116	Pegmatite dike	Ms, Bt, Chl, Kfs, Pl Qtz	Weakly deformed dike that extends from contact of BMP into marble; interpreted to possibly be latest F_2	Igneous Zrn = 171 ± 5 Ma, possibly constrains latest development of F_2	E 402100, N 5739050, 2260 m
DG129	Leucogranitic dike	Ms, Bt, Chl, Kfs, Pl Qtz	Undeformed vertical dike, highly discordant, truncates transposed fabrics and folds in host calc-silicate	Igneous Zrn = 169 ± 2 Ma, possibly as young as 163 ± 1 Ma; Post-dates deformation	E 402540, N 5738650, 2395 m
Domain 1: West flank of fan—Adamant					
DG169	Bt–Hbl granodiorite	Bt, Hbl, Kfs, Pl, Qtz, Hyp*, Aug*; *Px's mantled by Hbl	Coarse-grained; weak alignment of Hbl and Bt; margin highly discordant to regional structures (D_2), which is deflected around SW and NE corners of pluton; contact aureole overprints regional fabrics (Logan and Colpron, 1995)	Igneous Zrn ca. 171–167 Ma; wt. mn. = 167 ± 0.3 Ma; interpreted to constrain latest development of S_2 fabric and pre-D_3	E 422100, N 5727300, 2200 m
Domain 2: Transition zone (fan axis)—French Glacier area					
DG09	Medium-grained tonalite dike	Ms, Grt, Pl, Qtz	Folded and boudinaged dike, with axial planes parallel to S_2 transposition; somewhat discordant margins suggest transposition was ongoing when dike was emplaced	Igneous Zrn = 167 ± 3 Ma; syn-D_2 thermally overprinted at 91 ± 2 Ma, same age as Mnz in host pelitic schist	E 414710, N 5735940, 2040 m
DG02	Medium-grained tonalite dike	Bt, Ms, Chl, Pl, Qtz	Crosscutting dike with entrained xenoliths of transposed (S_2) pelitic schist; small apophyses appear to be slightly strained; subgrains and undulose extinction in Qtz and Pl in thin section	Igneous Mzn = 156 ± 0.6 Ma; youngest age constraint for D_2 in this area; however there appears to have been subsequent minor deformation (D_3?)	E 415160, N 5734820, 1865 m
Domain 2: Transition zone (fan axis)—Argonaut Mountain area					
DG70a	Pegmatite dike	Bt, Grt, Kfs, Pl, Qtz	Folded (F_3) pegmatite that is discordant to the transposition foliation (S_2)	Igneous Mnz = 104 ± 3 Ma; post-F_2, pre- to syn-D_3	E 410730, N 5738180, 2460 m
DG69	Tur–Grt–Bt–Ms pegmatite dike	Tur, Grt, Bt, Ms, Kfs, Pl, Qtz	Undeformed pegmatite that crosscuts both limbs of large (~20 m scale) F_3 folds; contains entrained xenoliths of foliated (S_2) country rock	Igneous Mnz = 81 ± 0.2 Ma; youngest age constraint for D_3 in this area	E 411300, N 5738125, 2470 m
Domain 3: East flank of fan—Mud Glacier area					
DG22c	Leucosome	Ms, Bt, Grt, Pl, Qtz	Folded (F_3) leucosome within a Sil–Grt–Bt pelitic schist; peak metamorphic minerals (Sil and Bt) in S_2 are folded and crenulated around hinge of the fold	Mnz = 104 ± 2 Ma (primary? interior) surrounded/overprinted by 97.1 ± 1.5 Ma (secondary exterior); Zrn = 92 ± 1 Ma interpreted as metamorphic overprint	E 400325, N 5755000, 2150 m
DG22b	Coarse-grained pegmatite	Tur, Ms, Pl, Kfs, Qtz	Essentially undeformed (thin section does show undulatory extinction and development of subgrains in Qtz); crosscuts all folds and fabrics in country rock; contains xenoliths of foliated (S_2) country rock	Mnz = 63 ± 1 Ma; interpreted as post-tectonic at this location	E 400350, N 5755000, 2150 m

Table 1 (*continued*)

Sample	Lithology[b]	Mineralogy[c]	Texture/fabric/structural interpretation	Interpreted age[d]	Location (UTM)
Domain 3: East flank—Warsaw Mountain area					
DG246	Medium-grained Qtz–diorite dike	Ms, Pl, Qtz	Folded (F_3) dike that is discordant to the transposition foliation (S_2); S_2 and associated leucosome folded around F_3 fold hinges in dike; contains xenoliths of foliated (S_2) country rock	Igneous Mnz = 92 ± 1 Ma with secondary overgrowth at 80 ± 1 Ma; primary (?) Zrn ca. 90 ± 2 Ma with secondary overgrowth at 76 ± 2 Ma; ages interpreted as post-D_2 (S_2), pre- to syn-D_3	E 402667, N 5763431, 2268 m
DG231	Medium-grained tonalite dike	Ms, Pl, Qtz	Dike crosscuts both limbs of two meter-scale F_3 folds; minerals are randomly oriented in thin section and hand sample, with only minor evidence for strain (e.g. undulatory extinction, minor subgrain development)	Mnz = 84 ± 0.2 Ma; age of dike interpreted to be post-F_3	E 402320, N 5764259, 2485 m

[a] Summary is presented in geographic order from southwest to northeast across the fan.
[b] Assignment of igneous rock lithology according to the IUGS classification system.
[c] Mineral abbreviations after Kretz (1983); only major rock forming minerals listed.
[d] Quoted monazite (Mnz) ages are based on $^{207}Pb/^{235}U$ (IDTIMS) or $^{208}Pb/^{232}Th$ (SHRIMP) isotopic ratios; zircon (Zrn) are based on $^{206}Pb/^{238}U$ isotopic ratio; wt. mn. = weighted mean.

development of the transposition fabric (S_2) in the area, consistent with plutons of similar age, composition and geologic setting ~50 km south, such as the ca. 168 Ma Pass Creek and Fang plutons (Brown et al., 1992; Colpron et al., 1996).

4.3.1.2. CT07—highly strained pegmatite (SHRIMP only). Sample CT07 is from an isoclinally folded muscovite–biotite bearing pre- to syn-D_2 pegmatite dike (Fig. 6a) that is hosted in marble approximately 1 km south of the Bigmouth pluton. The fold limbs are highly attenuated and dismembered, leaving rootless isoclinal hinges within the host marble. Axial planar foliation dips shallowly to the northeast, parallel to the regional S_2 transposition foliation. IDTIMS analyses were not carried out due to a paucity of zircon grains, which were mostly turbid and sugary, suggesting severe alteration (Zrn 8, Fig. 6d). Instead, three euhedral, crack- and inclusion-free zircon crystals and one altered zircon with clear tips were chosen for SHRIMP analyses. BSE images of the three relatively clear grains revealed diffuse oscillatory zoning around inherited cores (Zrn 1, 2 and 3, Fig. 6d). Two analyses in the cores yielded Late Archean (2933 ± 6 Ma) and Middle Proterozoic (1113 ± 41 Ma) ages (Fig. 6b), similar to the range found in inherited zircon cores from the Bigmouth pluton. The oscillatory zones surrounding the cores are interpreted to represent igneous growth during crystallization of CT07. Three SHRIMP analyses were targeted within the oscillatory zoning of Zrn1, 2 and 3, and a fourth in the tip of Zrn 8. The $^{206}Pb/^{238}U$ ages range between 171 ± 1 and 167 ± 1 Ma, with a weighted mean age of 169 ± 3 Ma. None of the analyses were concordant (Fig. 6c), but three overlapped concordia within error (1.3, 2.2, and 8.1). The discordance could be due to the spots overlapping the older cores, but this is not supported by the BSE images in Fig. 6d. Alternatively, the discordance may be the result of imprecise $^{207}Pb/^{235}U$ ages due to low ^{207}Pb counts; thus, the age is interpreted to be 169 ± 3 Ma based on the $^{206}Pb/^{238}U$ chronometer.

In the BSE images, the domains of oscillatory zoning in Zrn1, 2 and 3 appear to be partly resorbed and overgrown by brighter rims of homogeneous zircon (Fig. 6d). One SHRIMP spot placed entirely within the bright rim of Zrn1 yielded a $^{206}Pb/^{238}U$ age of 90.7 ± 1.4 Ma, coincident with metamorphic ages produced within Domains 2 and 3 of this study (Gibson, 2003). This is thought to represent a Late Cretaceous overprint, which has implications for the two normally discordant (~6–16%) titanite fractions of Marchildon (1999) that gave $^{206}Pb/^{238}U$ ages of 140.5 ± 0.8 and 137.4 ± 1.4 Ma. The titanite ages are re-interpreted to represent a mixture of primary Middle Jurassic titanite partially recrystallized or overgrown during an overprint at ca. 91 Ma, rather than reset during a second metamorphic event (M_2) at ca. 140 Ma. These data do not refute the sequence of metamorphic events proposed by Marchildon (1999), only their timing. More geochronology is required to examine the significance of the Late Cretaceous overprint and its relationship to M_2 of Marchildon (1999).

4.3.1.3. DG116—weakly folded pegmatite (IDTIMS and SHRIMP). DG116 comes from a muscovite–biotite-bearing pegmatite dike that extends from the contact of the Bigmouth pluton into the host marble (Fig. 7a), and is interpreted to be a late stage phase of the pluton. The dike is weakly folded, with axial planes that strike 332° and dip 44° to the northeast, which is concordant with the foliation in the host marble. The zircon grains chosen for IDTIMS analysis included two fractions (A, D) that were turbid and inclusion-

rich, and two U-rich fractions (B and C, ~2–5 wt% U; ES Table 1) that were clear and resinous brown with few inclusions. All but fraction A, a turbid, inclusion-rich, single-grain fraction, plotted above the concordia curve (Fig. 7b). Fraction A was closest to being concordant (3% discordant), with a $^{207}Pb/^{206}Pb$ age of 167±22 Ma. The isotopic composition of fractions B–D is enigmatic; the points are reversely discordant and lie on a line parallel to the $^{207}Pb/^{235}U$ axis. Interestingly, fractions B and C have $^{206}Pb/^{238}U$ ages within error of fraction A, suggesting that the $^{207}Pb/^{235}U$ isotopic system was disturbed either naturally or analytically.

Four SHRIMP analyses of four resinous brown zircon grains are normally discordant and lie along a discordia line that passes through the origin (Fig. 7b). A linear regression of the SHRIMP data and IDTIMS fraction A yields an upper intercept of 170.8±4.6 Ma, interpreted to be the approximate age of this weakly deformed pegmatite. The intersection of the discordia line with the origin suggests recent Pb loss that was likely enhanced by metamictization and fluid-mediated leaching along microfractures.

4.3.1.4. DG129—undeformed leucogranitic dike (IDTIMS and SHRIMP). This sample comes from an undeformed, crosscutting leucogranitic dike. Second generation folds and transposition foliation within the host calc-silicate are truncated by the highly discordant margins of the dike (Fig. 8a). In thin section, randomly oriented, euhedral to subhedral minerals with uniform extinction indicate no evidence of strain. IDTIMS analyses were carried out on multigrain fractions of clear, euhedral, prismatic crystals with few inclusions and no optically discernable cores. The data are normally discordant with $^{207}Pb/^{206}Pb$ ages between ca. 487 and 178 Ma (Fig. 8b; ES Table 1), clearly indicating inheritance. BSE images revealed the presence of cores surrounded by a diffuse oscillatory-zoned mantle (Fig. 8c). A discordia line through the data produced a lower intercept of 163±1 Ma (Fig. 8b), interpreted to reflect the igneous age of the dike, and an upper intercept of 2082±64 Ma that is attributed to inheritance. Four SHRIMP spots (2.1, 5.1, 7.1, and 13.1) within oscillatory-zoned domains of four zircon crystals overlap the concordia curve (Fig. 8c and 8d); the $^{206}Pb/^{238}U$ ages range between 171±1 and 167±4 Ma, with a weighted mean of 169±3 Ma, interpreted to represent the igneous age of the dike. The age of a fifth spot, 12.1, is clearly discordant, and although it is not clear in the BSE image, it must represent partial sampling of an older inherited core. The difference between the SHRIMP age of 169±2 Ma and the IDTIMS age of 163±1 Ma is enigmatic. Possibly the IDTIMS age has been influenced by the Late Cretaceous overprint that affected CT07, variable ages of inheritance, and/or recent Pb loss. However, a good linear fit for the discordia chord with a MSWD of 0.14 suggests otherwise. Thus, post-tectonic dike emplacement is considered to be as old as 169±2 Ma, but possibly as young as 163±1 Ma.

4.3.1.5. DG169—Adamant Pluton (IDTIMS and SHRIMP). In map view the Adamant pluton is an elliptical (~27 km × 6 km) east-trending intrusion (Figs. 1 and 3) that is cored by hypersthene–augite monzonite enclosed by quartz monzonite to hornblende–biotite granodiorite (Fox, 1969). The pluton is interpreted to be a single body (Fox, 1969; Shaw, 1980), which is highly discordant to the trend of regional D_2 structures that are deflected around the pluton's southwest and northeast margins (Shaw, 1980). Along the eastern margin, the pluton has a strong southwest-dipping foliation that is continuous with S_2 in the country rock (Fig. 9a). Near the west margin of the pluton where there is little evidence of post-emplacement strain (Fig. 9b), Shaw (1980) carried out IDTIMS U–Pb analyses on three multigrain fractions of zircon that yielded an average age of 169±4 Ma. This was thought to be the time of metamorphism rather than pluton emplacement, because zircon appears to be confined to the hydrated, outer zones of the pluton. However, Woodsworth et al. (1991) and Logan and Colpron (1995) interpreted the age as the time of emplacement based on mapping a contact aureole that overprinted regional fabrics near the southwest corner of the pluton.

In this study, four multigrain fractions of clear, euhedral, prismatic, and inclusion-free zircon from an unstrained portion of the pluton (Fig. 9b) near the western margin were analyzed by IDTIMS. The data cluster just below the concordia curve at 167 Ma (2–4% discordant; Fig. 9c); they have a weighted mean $^{206}Pb/^{238}U$ age of 166.8±0.3 Ma. The discordance is likely caused by the presence of very small xenocrystic cores that were not detected optically prior to the analysis, but were revealed in CL images of other similar zircon crystals. Eight SHRIMP analyses on four zircon grains yielded $^{206}Pb/^{238}U$ ages between 170 and 163 Ma (Fig. 9d). The CL images (Fig. 9e) displayed both straight, elongate zones and oscillatory zones. Both types of zircon are considered igneous based on their distinct zoning and euhedral habit. The four SHRIMP spots within these zones yielded $^{206}Pb/^{238}U$ ages between 170 and 166 Ma. Truncating the interior zones are discordant, fairly homogenous low-U zones (brighter CL zones equate to lower U and Th concentrations; Fig. 9e), which produced slightly younger and more discordant ages between 165 and 163 Ma (Fig. 9d). The increased discordance may be due to analyzing lower ^{207}Pb concentrations. These younger zones could also represent metamorphic recrystallization, but since they overlap within error the ages of the interior zones this cannot be demonstrated. The mean of all eight $^{206}Pb/^{238}U$ SHRIMP ages, 167±2 Ma, matches that for the IDTIMS analyses, 166.8±0.3 Ma, and is considered the igneous age of the late-syn-D_2 Adamant pluton.

4.3.2. Domain 2: transition zone—fan axis

4.3.2.1. DG09 (and DG01)—folded (F_2) tonalite dike, French Glacier (IDTIMS and SHRIMP). DG09 is a medium-grained tonalite dike with veins that are both

folded by F_2 and boudinaged (Fig. 10a). The near-vertical axial planes of the F_2 folds dip steeply to the south, concordant with the transposition fabric (S_2) in the host sillimanite–garnet–muscovite–biotite schist. Four multi-grain zircon fractions were analyzed by IDTIMS (Fig. 10c). Fractions A and B contained brownish-grey elongate and prismatic zircon with minor fractures, whereas fractions C and D were clear, elongate and prismatic. All data plot very close to 167 Ma, with fraction A being most concordant (-1% discordant) with ages of 167 ± 3 Ma for both the $^{206}Pb/^{238}U$ and $^{207}Pb/^{235}U$ ratios; this is interpreted to be the igneous age of this pre- to syn-F_2 dike. The very slight negative discordance is enigmatic; it cannot be attributed to excess ^{206}Pb since zircon incorporates relatively little Th when it crystallizes (see Schärer, 1984; Parrish, 1990). Nevertheless, the next most concordant analysis, fraction B (2.8% discordant), has a $^{206}Pb/^{238}U$ age of 166.4 ± 0.7 Ma, strongly suggesting that 167 ± 3 Ma is the correct age for this dike.

One SHRIMP spot on a monazite from this sample produced an age of 90 ± 1 Ma, which agrees with monazite ages from a nearby pelitic schist (DG01, Fig. 10b and c). This is thought to represent the time of a significant overprint, possibly M2 of Marchildon (1999). Anchoring a regression line from 90 Ma through zircon fractions A, B and D yields an upper intercept of 167 ± 9 Ma (Fig. 10c), which supports the interpretation that the igneous age of this dike is 167 Ma.

4.3.2.2. DG02—crosscutting tonalite dike, French Glacier (IDTIMS). DG02 is a tonalite dike that crosscuts the transposition foliation (S_2) and contains foliated xenoliths of the host sillimanite–garnet–muscovite–biotite schist (Fig. 10b), suggesting dike emplacement post-dated S_2. However, small apophyses extending from the dike margin appear to be weakly deformed, most likely by D_3. Two single-grain monazite fractions were analyzed by IDTIMS. Single-grain zircon fractions were analyzed, but the data were meaningless due to extremely low Pb content ($\sim$0.3–8.0 ppm). The monazite crystals analyzed were light yellow, clear, inclusion-free, with well-formed crystal faces that are indicative of igneous crystallization. BSE images of monazite from this sample display oscillatory zoning (Fig. 10c inset), consistent with an igneous origin. The two monazite fractions, M1 and M2, are nearly concordant (1.5 and 0.8% discordant, respectively), with essentially the same $^{207}Pb/^{206}Pb$ ages of 156 Ma. The most concordant fraction, M2, has a $^{207}Pb/^{235}U$ age of 155.5 ± 0.6 Ma, interpreted to be the igneous age of this post-D_2, pre-D_3 dike.

4.3.2.3. DG70a—folded (F_3) pegmatite dike, Argonaut Mountain (IDTIMS and SHRIMP). DG70a is a discordant garnet–muscovite pegmatite that truncates and entrains the S_2 transposition foliation in the host sillimanite–garnet–biotite–muscovite schist, but is folded by F_3 (Fig. 11a). The F_3 folds are disharmonic with close to tight hinges, and have axial surfaces that dip moderately ($\sim$50°) toward the northwest. Five single-grain monazite fractions were analyzed by IDTIMS. Zircon grains in this sample were too altered to be analyzed. The monazite crystals were pale yellow, clear, inclusion-free and had a subhedral habit. Four fractions, M2, M3, M4 and M6, with minimal normal and reverse discordance between 3.0 and -6.2%, plotted on the concordia curve at ca. 100 Ma, whereas fraction M5 with 10% normal discordance overlaps concordia at ca. 98 Ma (Fig. 11c). Monazite grains dated from the host pelitic schist (DG70b) produced a similar range of U–Pb ages (Gibson, 2003). Five SHRIMP spots within variably zoned monazite grains plotted on a U–Th–Pb concordia diagram between 106 and 102 Ma (Fig. 11d) with a $^{208}Pb/^{232}Th$ weighted mean age of 103.5 ± 2.7 Ma. The younger IDTIMS ages, especially for M5, likely resulted from analyzing igneous monazite with variable amounts of younger rims (e.g. Th map, Mnz4, Fig. 11e). Thus, the weighted mean SHRIMP age of 103.5 ± 2.7 Ma is interpreted as the igneous age of this pre- to syn-F_3 dike.

4.3.2.4. DG69—undeformed, crosscutting pegmatite (IDTIMS). DG69 is an undeformed, tourmaline–garnet–biotite–muscovite pegmatite dike that crosscuts both limbs of a 20-m-scale F_3 fold (Fig. 11b), and contains foliated (S_2) xenoliths of country rock. All zircon grains separated from this dike were too severely altered to analyze. Three single-grain monazite fractions were analyzed by IDTIMS (ES Table 1). The monazite crystals were light yellow, clear, inclusion-free, sub- to euhedral in habit, and show sector zoning in BSE images (Fig. 11c). The fractions are reversely discordant and plot in a tight cluster above 81 Ma on the concordia curve, which matches the $^{207}Pb/^{235}U$ age for all three fractions. Thus, the weighted mean $^{207}Pb/^{235}U$ age of 80.8 ± 0.2 Ma is considered to be the age of this post-D_3 dike.

4.3.3. Domain 3: east flank of fan

4.3.3.1. DG22c—folded (F_3) leucosome, Mud Glacier (IDTIMS). DG22c is a medium-grained muscovite–biotite–garnet–plagioclase–quartz-bearing leucosome within a sillimanite–garnet–biotite–muscovite schist. The leucosome is concordant with the south- to southwest-dipping ($\sim$60–80°) S_2 transposition foliation. Both the leucosome and S_2 have been folded and crenulated by F_3 (Fig. 12a), with a hinge that plunges 48° to the southeast and an axial plane that dips 48° to the south–southwest. Three clear, xenoblastic monazite grains were dated by IDTIMS. The fractions are spread out slightly above concordia between 93 and 91 Ma (Fig. 12b), which likely reflects a mixture of ages within single grains. Yttrium (Y) maps for two monazite grains (Fig. 12c) that were analyzed by the SHRIMP demonstrate at least two chemical domains. Two SHRIMP spots within the darker, lower Y interiors produced a slightly older age, 104 ± 2 Ma, compared with the lighter,

higher Y exterior domains that have a weighted mean $^{208}Pb/^{232}Th$ age of 97±2 Ma (Fig. 12d). It is unclear why the SHRIMP monazite ages for the higher Y exterior are older than those produced by IDTIMS, which interestingly match the SHRIMP zircon ages (see below) and monazite fractions analyzed from the host pelitic schist (DG23; Gibson, 2003). Nevertheless, the older 104±2 Ma, lower Y portion is interpreted to have grown during the earlier stages of prograde metamorphism. The 97±2 Ma, higher Y portion likely represents partial recrystallization during sillimanite-grade metamorphism and leucosome generation; the latter may be as young as ca. 92 Ma based on the IDTIMS ages and the SHRIMP analysis of zircon. BSE images of zircon display a diffuse, dark inner core surrounded by a lighter, fairly uniform mantle (Fig. 12c). Three zircon cores analyzed by the SHRIMP are Archean in age. Two spots within the mantles of Zrn10 and Zrn15 produced an age of 92±1 Ma (Fig. 12e). The transposition foliation (S_2) is interpreted to have progressively developed before and after leucosome production (i.e. >104 Ma). F_3 folding of the leucosome occurred sometime after 104 Ma, possibly after 92 Ma.

4.3.3.2. DG22b—undeformed, crosscutting pegmatite, Mud Glacier (IDTIMS). DG22b is from a coarse-grained tourmaline–muscovite bearing pegmatite dike that crosscuts all fabrics (i.e. S_2, F_3) in the host pelitic schist, as well as a foliated (S_2) pegmatite (Fig. 13a). Three medium yellow, clear, and inclusion free single-grain monazite fractions were analyzed by IDTIMS. Fraction M2 was euhedral, whereas M3 and M4 were sub- to anhedral. The data plot in a line above the concordia curve between 67 and 63 Ma ($^{207}Pb/^{235}U$ ages; Fig. 13b). The spread of the data indicate that there was a mixture of ages within the single-grain fractions as thermally activated volume diffusion Pb loss is not considered a possible mechanism. BSE images did not reveal the presence of cores, but sector and irregular nebulous zoning were observed (Fig. 13b). The youngest $^{207}Pb/^{235}U$ age of 63.0±0.6 Ma (M3) is interpreted to be least affected by inheritance, and thus considered the best estimate of post-tectonic dike emplacement.

4.3.3.3. DG246—folded (F_3) quartz–diorite dike, Warsaw Mountain (IDTIMS and SHRIMP). DG246 is a medium-grained quartz–diorite dike with similar field relationships to that described for DG70a. DG246 was folded by open F_3 folds (Fig. 14a), but truncates the S_2 foliation in the host kyanite–garnet–biotite–muscovite schist, and contains foliated xenoliths of the schist. The S_2 foliation and associated leucosome in the schist are folded and crenulated within the hinges of the folded dike (Fig. 14a). Thus, DG246 is post-S_2 and pre- to syn-F_3. Three multigrain zircon fractions were dated by IDTIMS. The zircon crystals were euhedral, elongate and prismatic, and clear with very few inclusions. The data plot on a line immediately below the concordia curve (Fig. 14b). A best-fit linear regression anchored at the origin produced a discordia chord with an upper intercept of 84.1±6.9 Ma (MSWD=5.5), which is the same within error as the IDTIMS monazite ages from this sample (see below). BSE images of zircon grains in Fig. 14c display a consistent pattern, where the interior is either oscillatory zoned, mottled, or both, and is surrounded by unzoned, homogeneous zircon. The diffuse and mottled pattern of the interior suggests that a strong thermal or hydrothermal overprint affected these zircon crystals, and likely resulted in variable degrees of secondary recrystallization. Thus, the upper intercept age quoted above is not considered to be meaningful especially in light of zircon SHRIMP analysis (Fig. 14c). Four SHRIMP spots within the four zircon cores produced a weighted mean $^{206}Pb/^{238}U$ age of 90±2 Ma, interpreted to reflect the igneous age of this dike. The outer, secondary portions of the zircon crystals yielded a weighted mean $^{206}Pb/^{238}U$ age of 76±2 Ma, interpreted to be the age of metamorphic recrystallization.

The monazite crystals analyzed by IDTIMS were large (+202 μm), clear, inclusion-free, and euhedral. All four fractions are reversely discordant and plot between 88 and 85 Ma (based on $^{207}Pb/^{235}U$ ages), indicative of mixing between at least two age domains. BSE and chemical maps of Mnz2, 3, 5 and 6 in Fig. 14d reveal pristine, sector-zoned interiors truncated and surrounded by a uniform rim. Twelve SHRIMP analyses, targeted mainly within six monazite cores, produced a tight cluster around a weighted mean $^{208}Pb/^{232}Th$ age of 92±1 Ma (Fig. 14d), which is the same within error as the analyzed zircon interiors (90±2 Ma). Thus, 92±1 Ma is considered to be the best approximation for the time of dike crystallization. The data from the monazite rims are also tightly clustered, with a $^{208}Pb/^{232}Th$ weighted mean age of 80±1 Ma; this is interpreted to be the time of secondary crystallization of monazite, which is slightly older than the ca. 76 Ma zircon rims. The contrast between altered zircon and pristine monazite grains suggests that the zircon crystals were more prone to alteration. Perhaps this is related to the chemistry of hydrothermal fluids that may have affected DG246, and/or the degree of metamictization of zircon versus monazite.

4.3.3.4. DG231—crosscutting, post-F_3 tonalite dike (IDTIMS). DG231 is a medium-grained muscovite–plagioclase–quartz tonalite dike that crosscuts two, meter-scale F_2 folds that are gently refolded by F_3 (Fig. 15a). However, the dike has been strained (late D_3?); thin section analysis revealed most grains have undulatory extinction (Qtz, Pl, Ms; abbreviations after Kretz (1983)), subgrains (Qtz), and deformation twins (Pl). Four single-grain IDTIMS analyses were carried out on two monazite and two xenotime fractions (Fig. 15b) consisting of large (+202 μm), pristine, clear, euhedral grains indistinguishable under the microscope. Two fractions, M1 and M4, are reversely discordant and have $^{207}Pb/^{235}U$ ages of 85.4±0.1 Ma and 84.0±0.2 Ma, respectively. The two normally discordant fractions, X2 and X3, are considered to be xenotime because

they have Th/U values of 0.09 and 0.08, respectively, whereas monazite typically has Th/U $\gg$ 1.0. Fractions X2 and X3 have $^{207}Pb/^{206}Pb$ ages of 88.8 $\pm$ 1.6 Ma and 82.8 $\pm$ 2.1 Ma, respectively. The discordance in the xenotime fractions is enigmatic; it may be due to Pb loss, recrystallization, or overgrowth. However, the $^{207}Pb/^{206}Pb$ ages of X2 and X3 closely match the $^{207}Pb/^{235}U$ ages of the monazite, so recent Pb loss seems plausible. Conversely, the spread in the monazite data is likely due to inheritance and/or secondary growth. The youngest, most reversely discordant monazite fraction, M4, at 84 $\pm$ 0.2 Ma is considered to be the best approximation for the age of this post-F_{2-3} dike, because it was seemingly least affected by inheritance, overgrowth, or Pb loss.

5. Discussion

5.1. Domain 1—Middle Jurassic D_2 with minor Late Cretaceous overprint

In Domain 1, on the west flank of the fan, D_2 structures and transposition foliation (S_2) are at least as old as ca. 172–167 Ma, which agree with time constraints documented further south (e.g. Brown et al., 1992; Colpron et al., 1996). However, a minor Late Cretaceous (91 $\pm$ 1 Ma) overprint affected the Bigmouth pluton area, which is also recorded $\sim$3 km south near Argonaut pass (AP; Fig. 3a), where muscovite and biotite provided $^{40}Ar/^{39}Ar$ cooling ages of 76 $\pm$ 0.8 Ma (M. Colpron, 1997, pers. comm.). In a similar geologic setting $\sim$60 km to the southeast, this overprint was not found in the area around the Fang pluton. Based on $^{40}Ar/^{39}Ar$ cooling ages of hornblende, biotite, and muscovite, Colpron et al. (1996) concluded that there was $>$10 km of exhumation by late Middle Jurassic time, and that the region remained at upper crustal levels to the present. Thus, in the Late Cretaceous the Bigmouth pluton was likely at a deeper crustal level than the Fang pluton. This appears to be supported by the difference in metamorphic grade immediately adjacent to the two plutons (Bigmouth = sillimanite; Fang = biotite–garnet), but more work is needed to confirm when sillimanite grew in the wall rocks of the Bigmouth pluton.

5.2. Domain 2—Middle Jurassic D_2 overprinted by Cretaceous D_3 and high-grade metamorphism

Domain 2, which includes the fan axis, is referred to as the Transition zone. The U–Th–Pb isotopic evidence constrains D_2 to be Middle to Late Jurassic, ca. 167–156 Ma, and D_3 to be ca. 104–81 Ma. In addition, there was a significant metamorphic overprint during the mid- to Late Cretaceous (ca. 100–92 Ma, Gibson, 2003). The intensity of the overprint was greater in Domain 2 than in Domain 1, likely due to Domain 2 being at a deeper crustal level in the Cretaceous based on its higher metamorphic grade at this time (Gibson, 2003). Furthermore, all leucocratic dikes sampled in Domain 1 are Middle Jurassic in age; the only exception was a SHRIMP spot on a zircon rim yielding a Late Cretaceous age (CT07). Although Jurassic dikes are present in Domain 2 (i.e. French Glacier), there are also abundant Cretaceous dikes (Argonaut Mountain) that indicate Cretaceous anatexis affected Domain 2, but not Domain 1.

5.3. Domain 3—Cretaceous reworking of D_2, development of D_3, and high-grade metamorphism

Pervasive mid- to Late Cretaceous strain and metamorphism occurred within the east flank of the fan, Domain 3, where the highest-grade rocks are situated. Within Domain 3 isotopic evidence for Middle Jurassic strain and metamorphism is absent, possibly due to pervasive recrystallization of the zircon and monazite during high-grade metamorphism in the Cretaceous. Conversely, the U–Th–Pb data provide excellent age constraints for the Cretaceous (ca. 104–84 Ma) development and/or reworking of S_2, and overprinting by F_3. The temporal and spatial coincidence of F_3 with the Purcell fault has led us to agree with Simony et al. (1980) that these more open, buckle-style folds may be kinematically related to thrusting on the Purcell fault.

5.4. The relationship between deformation and metamorphism across the Selkirk fan

Across the breadth of the Selkirk fan, metamorphism is interpreted to have been synchronous with, and to have slightly outlasted, D_2 regardless of when D_2 developed or was reworked, i.e. Middle Jurassic versus Cretaceous. Perhaps this can be explained in part by the accumulated strain energy built up during a transposition event and the inevitable process of recovery (Williams and Jercinovic, 2003), as long as cooling following deformation is not so rapid as to quench the mineral assemblage. Another contributing factor is that major transposition events require a certain amount of heating, and when coupled with the accumulated strain energy, induces annealing. If this is correct, each successive transposition event would result in the appearance of metamorphism outlasting deformation. Furthermore, if annealing led to substantial recrystallization, this may even wipe out or significantly obscure the older events.

5.5. The Adamant pluton conundrum

The Adamant pluton straddles the fan axis (Figs. 1 and 3), which is problematic because it sits in all three domains defined in this study (Fig. 3c). Igneous zircon from the west end of the pluton demonstrate Middle Jurassic emplacement. However, unpublished Late Cretaceous $^{40}Ar/^{39}Ar$ cooling ages for muscovite and biotite in wall rocks near the

southwestern contact of the pluton (M. Colpron, 1997, pers. comm.) indicate it was at moderate to shallow crustal depth in the Cretaceous. Unfortunately, there are no ages from the east end of the pluton where its margin is highly strained, concordant with southwest-dipping S_2 (Fig. 9a). At the current level of exposure, the strain observed in the pluton's east end (Domain 3) suggests it was slightly hotter and more ductile, i.e. at a deeper crustal level, in the Cretaceous than the west end (Domain 1), which contains little evidence of strain (Fig. 9b). Cretaceous, northeast-directed thrusting on the Purcell fault could have uplifted deeper levels of the pluton's east end relative to the west end. More work is required in and around the Adamant pluton to test these hypotheses.

5.6. Strain partitioning and evidence for Middle Jurassic development of north-east vergent D_2

The preservation of isotopic evidence for the oldest Middle Jurassic structures and metamorphism is restricted to the highest stratigraphic and structural levels with the lowest metamorphic grade. Conversely, evidence for a penetrative Early to Late Cretaceous overprint is best preserved in the fan axis (Domain 2) and the eastern flank (Domain 3) where the highest-grade rocks and the deepest structural levels are exposed. These observations suggest that penetrative Cretaceous strain and high-grade metamorphism were concentrated within hotter, deeper crustal levels that were exhumed in the Late Cretaceous within the fan's eastern flank.

North of this study in the Monashee Mountains (Figs. 1 and 3) Crowley et al. (2000) documented a similar transition. The oldest Middle Jurassic strain and metamorphism are best preserved in the lowest-grade rocks (biotite–garnet grade), that were presumably situated at the highest crustal levels in this area during Cordilleran orogenesis. Most of the Cretaceous to Tertiary ages are found in the highest-grade, deepest-level rocks. It is important to note that the study area for Crowley et al. (2000) is within the same panel of rocks as Domain 3 of our study, i.e. the eastern flank of the Selkirk fan. Although not explicitly stated by Crowley et al. (2000), their data indicate that northeast-vergent deformation within the fan's east flank occurred as early as the Middle Jurassic. Along strike to the north ($\sim$52°35′N), Reid (2003, and references therein) attributes the development of structural fans with southwest- and northeast-vergent folds to be Early to Middle Jurassic, which are progressively overprinted by Cretaceous deformation at deeper levels. Thus, the combined results of Crowley et al. (2000), Reid (2003) and Colpron et al. (1996), and our study suggest that southwest- and northeast-vergent structures of the Selkirk fan initially developed in Middle Jurassic time. Data from this study and in the northern Monashee Mountains (e.g. Sevigny et al., 1990; Scammell, 1993; Crowley et al., 2000) also demonstrate that the southwest-dipping S_2 fabric in the east flank was located at deep crustal levels during the Cretaceous to Tertiary, suggesting that D_2 structures in the east flank (Domain 3) are strongly diachronous (Middle Jurassic–Tertiary). Moreover, structural analysis of Simony et al. (1980) and Perkins (1983) and this study demonstrate that D_2 on the east flank always developed with northeast-vergent asymmetry. We contend that the initial northeast-verging Middle Jurassic S_2 foliation in Domain 3 was progressively or episodically reworked and recrystallized during the Cretaceous. This implies that S_2 in the east flank of the fan is a composite foliation that developed for >100 My.

5.7. Tectonic implications

The data in this study and that presented by Crowley et al. (2000), indicate that growth of the Selkirk fan initiated in the Middle Jurassic with coeval development of both southwest- and northeast-verging structures. In the Cretaceous the northeast flank of the fan was remobilized and partially exhumed as deeper level rocks flowed northeastward. At the latitude of the study area the fan is therefore a composite structure consisting of a southwest-verging panel on the western flank that was exhumed to a high structural level in the Jurassic and a northeast-verging panel that was not exhumed from middle crustal depths until the Late Cretaceous.

The timing of the Jurassic proto-fan seems to agree with the models of Price (1986), Brown et al. (1993) and Colpron et al. (1998), but only Price (1986) and Brown et al. (1993) argue for $\sim$coeval development of both sides of the fan. Although, none of these models consider a strongly diachronous Jurassic to Cretaceous evolution for the fan's eastern flank, we contend that the new data appear to be best accommodated within a modified version of the Brown et al. (1993) model. In the revised model, a proto-fan was formed in the Middle Jurassic (Fig. 16a) during the accretion of the

Fig. 16. (a)–(c) Conceptual model for the tectonic development of the Selkirk fan. (a) During the incipient stages of accretion of the Intermontane Superterrane in the Early to Middle Jurassic a proto-fan formed in the accretionary wedge above point (S) where oceanic or marginal basin lithosphere subducted beneath North America in a fashion similar to that modeled by Malavieille (1984) and Willet et al. (1993). (b) Continued Middle Jurassic convergence and growth of the fan resulted in the development of large-scale nappes (F1), followed by a pervasive overprint by F2 folds coeval with prograde metamorphism. Expansion of the orogenic wedge was accompanied by the decoupling of the fan along a basal thrust system, resulting in its northeastward translation. Progressive thickening of the wedge led to the establishment of a plateau, beneath which a hot, ductile lower crustal zone developed and migrated eastward. (c) Mid-Cretaceous accretion of the Insular Superterrane resulted in out-of-sequence deformation in the leading edge of the retrowedge. Deeper-seated rocks in the central and east flanks of the fan were uplifted and exhumed along the Purcell thrust.

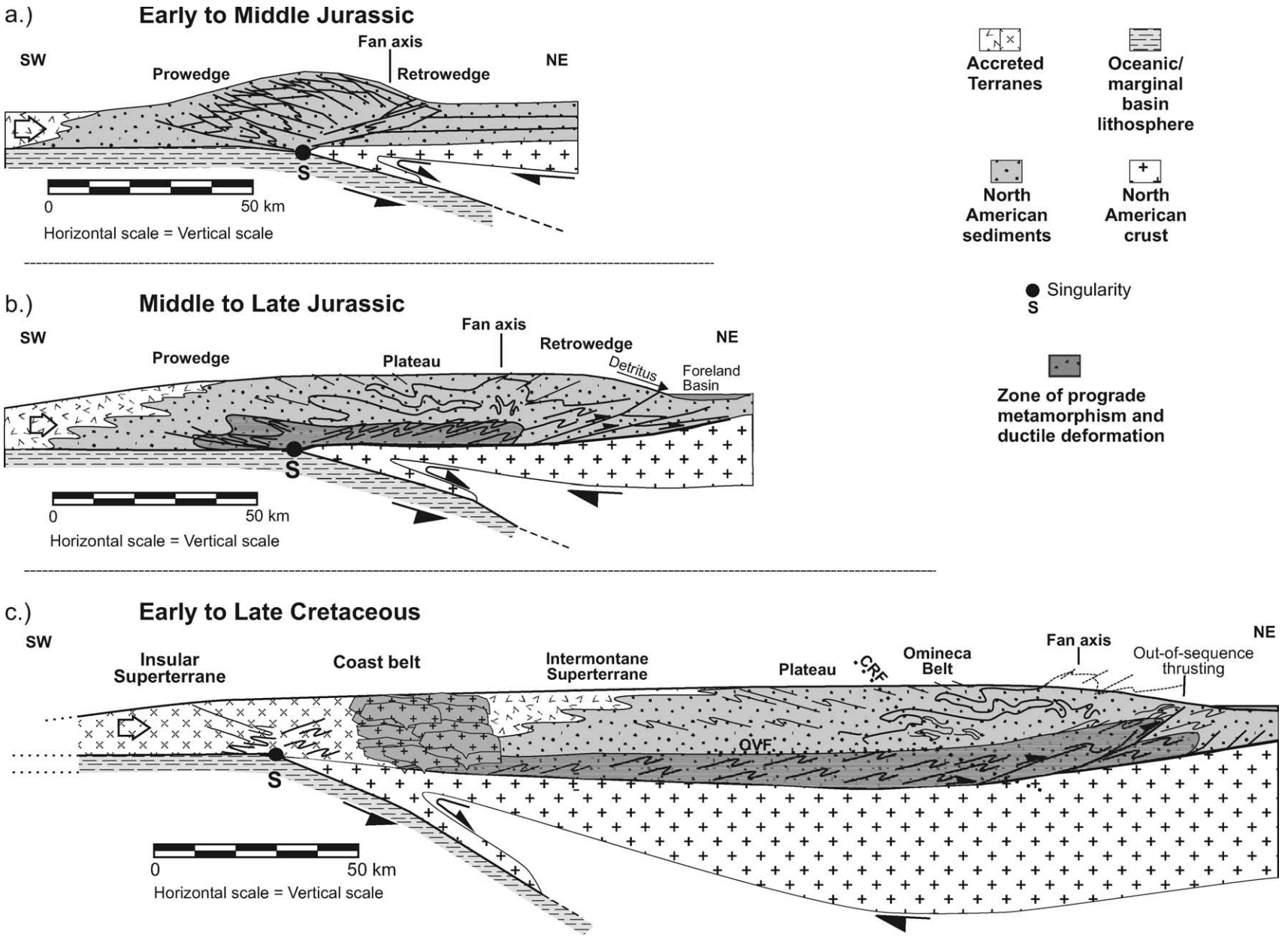

Figure 16 (*legend on previous page*)

Intermontane Superterrane (Monger et al., 1982; Murphy et al., 1995). As the fan expanded eastward, it became decoupled from its point of origin (i.e. subduction zone) and was translated toward the northeast (Fig. 16b). The Jurassic structures at high crustal levels remained unaffected, but deeper levels were reworked as material to the east was progressively accreted beneath the burgeoning orogenic wedge (see Brown, 2004). Continued eastward expansion, underthrusting and concomitant crustal thickening may have led to the establishment of a high plateau, beneath which a middle-crustal zone of hot and ductile rock developed. During the mid- to Late Cretaceous accretion of the Insular Superterrane, we suggest that a portion of the infrastructure was exhumed within the eastern flank of the Selkirk fan, brought up by out-of-sequence thrusting on the Purcell fault (Fig. 16c). This model and its tectonic implications will be presented in detail in future communications (Gibson et al., in review; Brown and Gibson, accepted), and have been presented in abstracts elsewhere (Brown and Gibson, 2003; Gibson et al., 2003).

6. Conclusions

New data provide U–Th–Pb geochronologic constraints for deformation associated with the development of the Selkirk fan. The data suggest that there has been juxtaposition of higher structural levels with an older deformation history in the west flank relative to lower levels that record a younger deformation history in the east. Dated monazite and zircon from variably deformed leucocratic dikes and plutons indicate that the thermo-structural development of the fan's west flank occurred principally in the Middle Jurassic (ca. $\geq$172–167 Ma). In contrast, data from east of the fan axis demonstrate that there has been substantial Early to Late Cretaceous (ca. 104–84 Ma) deformation superimposed on an earlier Middle Jurassic transposition fabric, and that significant exhumation did not occur until the Late Cretaceous. Thus, the Selkirk fan should be thought of as a composite structure of Middle Jurassic and Cretaceous strain, rather than a singular fan that developed during one progressive event.

Acknowledgements

This project was funded by NSERC grants held by Sharon Carr and Richard Brown. The J.C. Roddick Ion Microprobe Lab at the GSC provided excellent assistance in the acquisition of the U–Th–Pb SHRIMP data. The UMASS microprobe lab is thanked for the Y–Th–U X-ray mapping of monazite. The manuscript benefited from discussions with Philip Simony, Edward Ghent, James Crowley, Raymond Price and Michael Williams. Reviews by Maurice Colpron and Rebecca Jamieson significantly improved the quality of the manuscript.

Appendix. Supplementary Material

Supplementary data associated with this article can be found, in the online version, at doi:10.1016/j.jsg.2005.05.014

References

Braun, I., Montel, J.-M., Nicollet, C., 1998. Electron microprobe dating of monazites from high-grade gneisses and pegmatites of the Kerala khondalite belt, southern India. Chemical Geology 146, 65–85.

Brown, R.L., 1991. Geological map and cross section, Downie Creek map area (82M/8), British Columbia. Geological Survey of Canada Map 244, scale 1:50,000.

Brown, R.L., 2004. Thrust belt accretion and hinterland underplating of orogenic wedges: an example from the Canadian Cordillera. In: McClay, K.R. (Ed.), Thrust Tectonics and Hydrocarbon Systems AAPG Memoir 82, pp. 51–64.

Brown, R.L., Gibson, H.D., 2003. Comparison of Himalayan and Cordilleran tectonic processes. In: Geological Association of Canada/Mineralogical Association of Canada, Abstracts with Programs, 28.

Brown, R.L., Gibson, H.D., accepted. An argument for channel flow in the southern Canadian Cordillera and comparison with Himalayan tectonics. Geological Society of London Special Publication.

Brown, R.L., Lane, L.S., 1988. Tectonic interpretation of west-verging folds in the Selkirk Allochthon of the southern Canadian Cordillera. Canadian Journal of Earth Sciences 25, 292–300.

Brown, R.L., Tippett, C.R., 1978. The Selkirk fan structure of the southeastern Canadian Cordillera. Geological Society of America Bulletin 89, 548–558.

Brown, R.L., Tippett, C.R., Lane, L.S., 1978. Stratigraphy, facies changes, and correlations in the northern Selkirk Mountains, southern Canadian Cordillera. Canadian Journal of Earth Sciences 15, 1129–1140.

Brown, R.L., Lane, L.S., Psutka, J.F., Read, P.B., 1983. Stratigraphy and structure of the western margin of the Northern Selkirk Mountains: Downie Creek map area, British Columbia. Geological Survey of Canada, Paper 83-1A, pp. 203–206.

Brown, R.L., McNicoll, V.J., Parrish, R.R., Scammell, R.J., 1992. Middle Jurassic plutonism in the Kootenay Terrane, Northern Selkirk Mountains, British Columbia. Geological Survey of Canada, Paper 91-2, pp. 135–141.

Brown, R.L., Beaumont, C., Willett, S.D., 1993. Comparison of the Selkirk fan structure with mechanical models: implications for interpretation of the southern Canadian Cordillera. Geology 21, 1015–1018.

Campbell, R.B., 1968. Canoe River (83D), British Columbia. Geological Survey of Canada Map 15-1967, scale 1:253,440.

Cherniak, D.J., Watson, E.B., 2000. Pb diffusion in zircon. Chemical Geology 172, 5–24.

Cherniak, D.J., Watson, E.B., Grove, M., Harrison, T.M., 2002. Pb diffusion in Monazite. In: Geological Society of America Abstracts with Programs 34, 138-5.

Cocherie, A., Legendre, O., Peucat, J.J., Kouamelan, A.N., 1998. Geochronology of polygenetic monazites constrained by in situ electron microprobe Th–U–total lead determination: implications for lead behaviour in monazite. Geochimica et Cosmochimica Acta 62, 2475–2497.

Colpron, M., Logan, J.M., Gibson, G., Wild, C.J., 1995. Geology and mineral occurrences of the Goldstream River Area, Northern Selkirk Mountains (82M/9 and part of 10). British Columbia Ministry of Energy, Mines and Petroleum Resources Map 1995-2, scale 1:50,000.

Colpron, M., Price, R.A., Archibald, D.A., Carmichael, D.M., 1996. Middle Jurassic exhumation along the western flank of the Selkirk fan structure:

thermobarometric and thermochronometric constraints from the Illecillewaet synclinorium, southeastern British Columbia. Geological Society of America Bulletin 108, 1372–1392.

Colpron, M., Warren, M.J., Price, R.A., 1998. Selkirk fan structure, southeastern Canadian Cordillera: tectonic wedging against an inherited basement ramp. Geological Society of America Bulletin 110, 1060–1074.

Coney, P.J., 1980. Cordilleran metamorphic core complexes: an overview. Geological Society of America Memoir 153, 7–31.

Cook, F.A., Varsek, J.L., Clowes, R.M., Kanasewich, E.R., Spencer, C.S., Parrish, R.R., Brown, R.L., Carr, S.D., Johnson, B.J., Price, R.A., 1992. Lithoprobe crustal reflection cross section of the southern Canadian Cordillera, 1. Foreland thrust and fold belt to Fraser River fault. Tectonics 11, 12–35.

Crowley, J.L., Brown, R.L., 1994. Tectonic links between the Clachnacudainn terrane and Selkirk allochthon, southern Omineca Belt, Canadian Cordillera. Tectonics 13, 1035–1051.

Crowley, J.L., Ghent, E.D., 1999. An electron microprobe study of the U–Th–Pb systematics of metamorphosed monazite: the role of Pb diffusion versus overgrowth and recrystallization. Chemical Geology 157, 285–302.

Crowley, J.L., Ghent, E.D., Carr, S.D., Simony, P.S., Hamilton, M.A., 2000. Multiple thermotectonic events in a continuous metamorphic sequence, Mica Creek area, southeastern Canadian Cordillera. Geological Materials Research 2, 1–45.

DeWolf, C.P., Belshaw, N.S., O'Nions, R.K., 1993. A metamorphic history from micron-scale $^{207}Pb/^{206}Pb$ chronometry of Archean monazite. Earth and Planetary Science Letters 120, 207–220.

Digel, S.G., Ghent, E.D., Carr, S.D., Simony, P.S., 1998. Early Cretaceous kyanite–sillimanite metamorphism and Paleocene sillimanite overprint near Mount Cheadle, southeastern British Columbia: geometry, geochronology, and metamorphic implications. Canadian Journal of Earth Sciences 35, 1070–1087.

Dodson, M.H., 1973. Closure temperature in cooling geochronological and petrological systems. Contributions to Mineralogy and Petrology 40, 259–274.

Foster, G., Gibson, H.D., Parrish, R.R., Horstwood, M., Fraser, J., Tindle, A., 2002. Textural, chemical and isotopic insights into the nature and behaviour of metamorphic monazite. Chemical Geology 191, 183–207.

Fox, P.E., 1969. Petrology of Adamant pluton, British Columbia. British Columbia Department of Energy, Mines and Resources, Paper 67-61, pp. 1–101.

Gabrielse, H., Campbell, R.B., 1991. Upper Proterozoic assemblages, Chapter 6. In: Gabrielse, H., Yorath, C.J. (Eds.), Geology of the Cordilleran Orogen in Canada Geological Survey of Canada, Geology of Canada, no. 4, pp. 125–150.

Gerasimoff, M.D., 1988. The Hobson lake pluton, Cariboo Mountains, and its significance to Mesozoic and Early Tertiary Cordilleran tectonics. MSc thesis, Queen's University.

Ghent, E.D., Simony, P.S., Mitchell, W., Perry, D., Robbins, D., Wagner, J., 1977. Structure and metamorphism in the southeast Canoe River area, British Columbia. Geological Survey of Canada, Paper 77-1C.

Gibson, H.D., 2003. Structural and thermal evolution of the northern Selkirk Mountains, southeastern Canadian Cordillera: tectonic development of a regional-scale composite structural fan. PhD thesis, Carleton University.

Gibson, H.D., Brown, R.L., Carr, S.D., 2003. Tectonic evolution of the Selkirk Fan: a composite Middle Jurassic–Cretaceous structure, Northern Selkirk Mountains, Southeastern Canadian Cordillera. Geological Association of Canada/Mineralogical Association of Canada, Abstracts with Programs 28, A-401.

Gibson, H.D., Carr, S.D., Brown, R.L., Hamilton, M.A., 2004. Correlations between chemical and age domains in monazite, and metamorphic reactions involving major pelitic phases: an integration of ID-TIMS and SHRIMP geochronology with Y–Th–U X-ray mapping. Chemical Geology 211, 237–260.

Gibson, H.D., Brown, R.L., Carr, S.D., in review. Tectonic evolution of the Selkirk fan, northern Selkirk Mountains, southeastern Canadian Cordillera: a composite Middle Jurassic–Cretaceous structure. Tectonics.

Hanchar, J.M., Miller, C.F., 1993. Zircon zonation patterns as revealed by cathodoluminescence and backscattered electron images: implications for interpretation of complex crustal histories. Chemical Geology 110, 1–13.

Kretz, R., 1983. Symbols for rock-forming minerals. American Mineralogist 68, 277–279.

Krogh, T.E., 1982. Improved accuracy of U–Pb ages by the creation of more concordant systems using an air abrasion technique. Geochimica et Cosmochimica Acta 46, 637–649.

Leatherbarrow, R.W., 1981. Metamorphism of pelitic rocks from the northern Selkirk Mountains, southeastern British Columbia. PhD thesis, Carleton University.

Logan, J.M., Colpron, M., 1995. Northern Selkirk Project—Geology of the Goldstream River area (82M/9 and parts of 82M/10). British Columbia Geological Survey of Canada, Paper 1995-1, pp. 215–241.

Logan, J.M., Friedman, R.M., 1997. U–Pb ages from the Selkirk allochthon, Seymour Arm map area, southeast British Columbia (82M/8 and 9). British Columbia Geological Survey of Canada, Paper 1997-1, pp. 17–23.

Malavieille, J., 1984. Modélisation expérimentale des chevauchements imbriqués: Application aux chaînes de montagnes. Bulletin de la Société Géologique de France 26, 129–138.

Marchildon, M.N., 1999. Petrologic studies of process interactions in metamorphic systems: deformation and metamorphism in the Selkirk allochthon orogenic wedge; and feedback mechanisms during reactive fluid flow. PhD thesis, University of British Columbia.

Monger, J.W.H., Price, R.A., Tempelman-Kluit, D.J., 1982. Tectonic accretion and the origin of the two major metamorphic and plutonic welts in the Canadian Cordillera. Geology 10, 70–75.

Murphy, D.C., van der Heyden, P., Parrish, R.R., Klepacki, D.W., McMillan, W., Struik, L.C., Gabites, J., 1995. New geochronological constraints on Jurassic deformation of the western edge of North America, southeastern Canadian Cordillera. In: Miller, D.M., Busby, C. (Eds.), Jurassic Magmatism and Tectonics of the North American Cordillera Geological Society of America Special Paper 299, pp. 159–171.

Parrish, R.R., 1987. An improved micro-capsule for zircon dissolution in U–Pb geochronology. Chemical Geology 66, 99–102.

Parrish, R.R., 1990. U–Pb dating of monazite and its application to geological problems. Canadian Journal of Earth Sciences 27, 1431–1450.

Parrish, R.R., 1995. Thermal evolution of the southeastern Canadian Cordillera. Canadian Journal of Earth Sciences 32, 1618–1642.

Parrish, R.R., Krogh, T.E., 1987. Synthesis and purification of ^{205}Pb for U–Pb geochronology. Chemical Geology 66, 103–110.

Parrish, R.R., Roddick, J.C., Loveridge, W.D., Sullivan, R.W., 1987. Uranium–lead analytical techniques at the geochronology laboratory. Geological Survey of Canada, Paper 87-2, pp. 3–7.

Parrish, R.R., Carr, S.D., Parkinson, D.L., 1988. Eocene extensional tectonics and geochronology of the southern Omineca belt, British Columbia and Washington. Tectonics 7, 181–212.

Perkins, M.J., 1983. Structural geology and stratigraphy, Big Bend of the Columbia River, Selkirk Mountains, British Columbia. PhD thesis, Carleton University.

Pidgeon, R.T., 1992. Recrystallization of oscillatory zoned zircon: some geochronological and petrological implications. Contributions to Mineralogy and Petrology 110, 463–472.

Poulton, T.P., Simony, P.S., 1980. Stratigraphy, sedimentology, and regional correlation of the Horsethief Creek Group (Hadrynian, Late Precambrian) in the northern Purcell and Selkirk Mountains, British Columbia. Canadian Journal of Earth Sciences 17, 1708–1724.

Price, R.A., 1986. The southeastern Canadian Cordillera: thrust faulting, tectonic wedging, and delamination of the lithosphere. Journal of Structural Geology 8, 239–254.

Price, R.A., 1994. Cordilleran tectonics and the evolution of the western Canadian sedimentary basin, Chapter 2. In: Mossop, G., Shetsin, I. (Eds.), Geological Atlas of the Western Canadian Sedimentary Basin, pp. 13–24.

Price, R.A., Mountjoy, E.W., 1970. Geological structure of the Canadian Rocky Mountains between Bow and Athabasca Rivers—a progress report. In: Wheeler, J.O. (Ed.), Structure of the Southern Canadian Cordillera Geological Association of Canada, Special Paper 6, pp. 7–25.

Raeside, R.P., Simony, P.S., 1983. Stratigraphy and deformational history of the Scrip Nappe, Monashee Mountains, British Columbia. Canadian Journal of Earth Sciences 20, 639–650.

Read, P.B., Brown, R.L., 1979. Inverted stratigraphy and structures, Downie Creek, southern British Columbia. Geological Survey of Canada, Paper 79-1A, pp. 33–34.

Read, P.B., Brown, R.L., 1981. Columbia River fault zone: southeastern margin of the Shuswap and Monashee complexes, southern British Columbia. Canadian Journal of Earth Sciences 18, 1127–1145.

Reid, L., 2003. Stratigraphy, structure, petrology, geochronology and geochemistry of the Hobson Lake area (Cariboo Mountains, British Columbia) in relation to the tectonic evolution of the southern Canadian Cordillera. PhD thesis, University of Calgary.

Roddick, J.C., 1987. Generalized numerical error analysis with applications to geochronology and thermodynamics. Geochimica et Cosmochimica Acta 51, 2129–2135.

Roddick, J.C., Loveridge, W.D., Parrish, R.R., 1987. Precise U/Pb dating of zircon at the sub-nanogram Pb level. Chemical Geology 66, 111–121.

Scammell, R.J., 1993. Mid-Cretaceous to Tertiary thermotectonic history of former mid-crustal rocks, southern Omineca belt, Canadian Cordillera. PhD thesis, Queen's University.

Schärer, U., 1984. The effect of initial ^{230}Th disequilibrium on young U–Pb ages: the Makalu case, Himalaya. Earth and Planetary Science Letters 67, 191–204.

Sevigny, J.H., Parrish, R.R., Ghent, E.D., 1989. Petrogenesis of peraluminous granites, Monashee Mountains, southeastern Canadian Cordillera. Journal of Petrology 30, 557–581.

Sevigny, J.H., Parrish, R.R., Donelick, R.A., Ghent, E.D., 1990. Northern Monashee Mountains, Omineca Crystalline Belt, British Columbia: timing of metamorphism, anatexis, and tectonic denudation. Geology 18, 103–106.

Shaw, D.A., 1980. Structural setting of the Adamant pluton, Northern Selkirk Mountains, British Columbia. PhD thesis, Carleton University.

Simony, P.S., Ghent, E.D., Craw, D., Mitchell, W., Robbins, D.B., 1980. Structural and metamorphic evolution of the northeast flank of Shuswap complex, southern Canoe River area, British Columbia. Geological Society of America Memoir 153, 445–461.

Steiger, R.H., Jäger, E., 1977. Subcommission on geochronology: convention on the use of decay constants in geo- and cosmochronology. Earth and Planetary Science Letters 36, 359–362.

Stern, R.A., 1997. The GSC Sensitive High Resolution Ion Microprobe (SHRIMP): analytical techniques of zircon U–Th–Pb age determinations and performance evaluation. Geological Survey of Canada, Current Research 1997-F, pp. 1–31.

Stern, R.A., Berman, R.G., 2000. Monazite U–Pb and Th–Pb geochronology by ion microprobe, with an application to in situ dating of an Archean metasedimentary rock. Chemical Geology 172, 113–130.

Stern, R.A., Sanborn, N., 1998. Monazite U–Pb and Th–Pb geochronology by high-resolution secondary ion mass spectrometry. Geological Survey of Canada, Current Research 1998-F, pp. 1–18.

Vavra, G., 1990. On the kinematics of zircon growth and its petrogenetic significance: a cathodoluminescence study. Contributions to Mineralogy and Petrology 106, 90–99.

Wheeler, J.O., 1963. Rogers Pass map-area, British Columbia and Alberta (82N West Half). Geological Survey of Canada, Paper 62-32, pp. 1–32.

Wheeler, J.O., 1965. Big Bend map-area, British Columbia. Geological Survey of Canada, Paper 64-32, pp. 1–37.

Wheeler, J.O., McFeely, P., 1991. Tectonic assemblage map of the Canadian Cordillera and adjacent parts of the United States of America. Geological Survey of Canada Map 1712A, scale 1:2,000,000.

Willett, S., Beaumont, C., Fullsack, P., 1993. Mechanical model for the tectonics of doubly vergent compressional orogens. Geology 21, 371–374.

Williams, M.L., Jercinovic, M.J., 2003. Interactions between deformation and metamorphism; new techniques for interpreting *P–T* paths from metamorphic rocks. In: Geological Society of America Abstracts with Programs 35, 90.

Williams, M.L., Jercinovic, M.J., Terry, M.P., 1999. Age mapping and dating of monazite on the electron microprobe: deconvoluting multistage tectonic histories. Geology 27, 1023–1026.

Woodsworth, G.J., Anderson, R.G., Armstrong, R.L., 1991. Plutonic regimes, Chapter 15. In: Gabrielse, H., Yorath, C.J. (Eds.), Geology of the Cordilleran orogen in Canada Geological Survey of Canada, Geology of Canada, no. 4, pp. 491–531.

Zen, E., Hammarstrom, J.M., 1984. Magmatic epidote and its petrologic significance. Geology 12, 515–518.

Zhu, X.K., O' Nions, R.K., 1999. Zonation of monazite in metamorphic rocks and its implications for high temperature thermochronology: a case study from the Lewisian terrain. Earth and Planetary Science Letters 171, 209–220.

Zhu, X.K., O'Nions, R.K., Belshaw, N.S., Gibb, A.J., 1997. Significance of in situ SIMS chronometry of zoned monazite from the Lewisian granulites, northwest Scotland. Chemical Geology 135, 35–53.